Transmission and localisation in ordered and randomly-perturbed structured flexural systems

Giorgio Carta[a,b], Michele Brun[b], Alexander B. Movchan[a,*], Tetiana Boiko[a]

[a] *Department of Mathematical Sciences, University of Liverpool, L69 3BX Liverpool, UK*
[b] *Dipartimento di Ingegneria Meccanica, Chimica e dei Materiali, Università di Cagliari, Piazza d'Armi, 09123 Cagliari, Italy*

Abstract

The paper presents a novel analysis of localisation and transmission properties of randomly-perturbed flexural systems. Attention is given to the study of propagation regimes and the connection with localised resonance modes in the context of Anderson's localisation. The analytical study is complemented with numerical simulations relevant to the design of efficient vibration isolation systems.

Keywords:
elastic discrete systems, random perturbations, transmission properties, localisation, transfer matrix, eigenvalue problem

1. Introduction

1.1. Periodic versus perturbed structures

Many structures are designed as assemblies of identical units, connected to each other with different kinds of joints. Such structures behave as filtering systems, since in some ranges of frequencies waves propagate without attenuation (if damping is neglected), while in others waves decay exponentially. For an infinite periodic system, these frequency ranges are denoted as *pass-bands* and *stop-bands*, respectively. A finite system exhibits similar

*Corresponding author
Email addresses: giorgio_carta@unica.it (Giorgio Carta), mbrun@unica.it (Michele Brun), abm@liverpool.ac.uk (Alexander B. Movchan), t.boiko@liverpool.ac.uk (Tetiana Boiko)

(a) (b)

Figure 1: (a) Oil storage tanks in a power generation plant (from http://www.chromalox.com, accessed on 30 July 2015); (b) failure of the San Saba bridge in Texas, occurred in May 2013 due to fire (image captured on 30 July 2015 from the video https://www.youtube.com/watch?v=LLVKb1HxhAY). (Online version in colour.)

transmission properties, provided that the number of its components is large enough. For a finite system, we distinguish between *propagation ranges* and *non-propagation ranges* since, strictly speaking, the definitions of pass-bands and stop-bands cannot be adopted.

Real structures are never perfect, as errors in manufacturing processes are likely to occur. The presence of defects and imperfections in the geometric and constitutive properties of the structure is generally referred to as "disorder". Disordered systems consisting of many units can be found at different scales, from photonic crystals at the nanoscale to mechanical and civil engineering structures at the macroscale. In this paper, we focus the attention on elastic media that can be modelled as discrete systems. For instance, arrays of tanks (Fig. 1a) can be studied as chains of masses connected by flexural links, which simulate the elastic plate supporting the tanks. In this case, disorder can be represented by the randomly-varying amount of fluid inside the containers. Bridges can be studied as discrete sets of masses connected by non-inertial beams and resting on elastic supports, as in the analytical model developed by Brun, Giaccu, Movchan, & Slepyan (2014) to describe the recent collapse of the San Saba bridge in Texas (Fig. 1b). In the case of bridges, the random parameters could be the span lengths or the pillar heights.

Systems made of modular units can be classified according to the number of kinematic variables p defining the coupling between two adjacent units: *mono-coupled* if $p = 1$, *bi-coupled* if $p = 2$, and so on. The dynamic proper-

ties of mono-coupled disordered systems have been extensively investigated in the literature. Sigalas & Soukoulis (1995), Cetinkaya (1999), Li, Wang, Hu, & Huang (2006), Chen & Wang (2007), Guenneau, Movchan, Movchan, & Trebicki (2008), Asatryan, Gredeskul, Botten, Byrne, Freilikher, Shadrivov, McPhedran, & Kivshar (2010), Asatryan, Botten, Byrne, Freilikher, Gredeskul, Shadrivov, McPhedran, & Kivshar (2012) studied propagation of elastic waves with different angles of incidence in disordered layered structures, where the quantity undergoing a random perturbation is the thickness of the layers, the elastic constant of one phase or the sequence of the layers. The effect of disorder in continuous one-dimensional randomly-perturbed systems is described by Godin (2005) with the analysis of the Lyapunov exponent for exponentially decaying perturbations, and by Godin, Molchanov, & Vainberg (2011) by examining the dependence of the Lyapunov exponent on the frequency and on the magnitude of disorder. A simple mass-spring model is employed by Yan, Zhang, & Wang (2009) to analyse localised modes in a layered structure after introducing different sources of disorder. In the context of bi-coupled systems, Ariaratnam & Xie (1995), Bouzit & Pierre (2000), Li, Wang, Hu, & Huang (2004) investigated different aspects of wave localisation in continuous beams, resting on many supports and having random span length, using the notion of *localisation factor*, which is related to the Lyapunov exponents of the dynamic system. For a general discussion on localisation phenomena in engineering structures, the reader is referred to the review by Bendiksen (2000).

In this paper, we describe spectral and transmission properties of discrete flexural systems with random parameters, and we make a comparison with the properties of perfect systems. In particular, we discuss localisation of eigenvectors and eigenvalues of matrices with random entries, derived from the equations of motion of the disordered system, in the framework of a generalised notion of Anderson's localisation (Anderson (1958)). We show that in a perturbed system localised resonance modes appear (Fig. 2a), while in a perfect system the eigenstates are spread over the entire structure (Fig. 2b). Isolated eigenvalues are detected in the spectrum of the perturbed system, especially near its boundaries (Fig. 2a). We demonstrate that there is a link between the eigenvalue problem and the energy transmission problem, since at the frequencies where localised modes are observed all the energy transferred to the system by an external source is reflected back. We verify the above results by computing also the localisation factor, which defines the decay rate of the wave amplitudes.

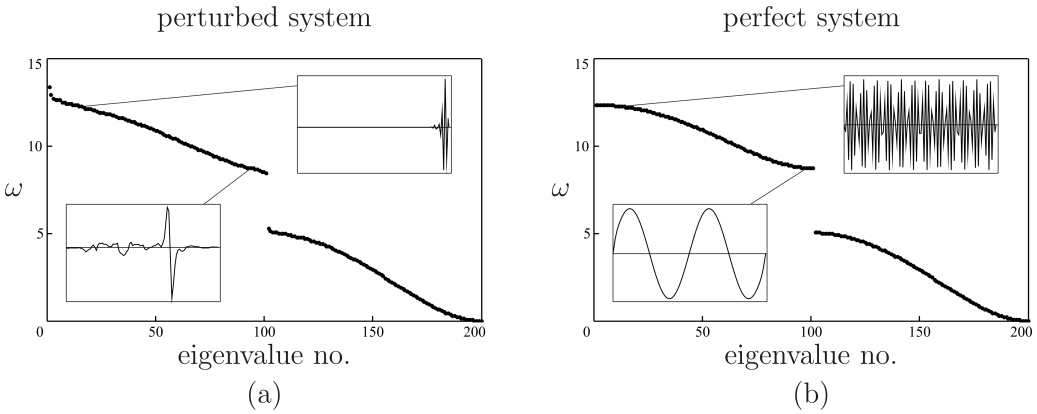

Figure 2: Eigenfrequencies ω and examples of eigenvectors of a finite discrete flexural system, consisting of disks connected by massless beams, in the case of perturbed conditions (a) and in the perfect configuration (b).

1.2. Anderson's localisation in discrete systems

Strong dynamic localisation. There are two classes of mathematical models of disordered systems in the modern physics: continuous and discrete. The continuous models are described, for example, by the Schrödinger equation with a random potential, while the discrete models are based on the random matrix of the Hamiltonian. The Schrödinger equation is a partial differential equation that determines the wave functions of the system and describes their changes with time. In the Copenhagen interpretation of quantum mechanics, the squared modulus of the wave function, $|\varphi|^2$, is proportional to the probability of finding the particle at that point. Another postulate of quantum mechanics is that observables are represented by linear Hermitian operators which act on the wave function, and the eigenvalues of the operators correspond to the possible values the observables take (Griffiths (2004)).

In the discrete case, one of the most important properties of disordered systems is the possible appearance of localised states. The wave functions of such states may vary significantly in some domains of a finite volume. In his remarkable work P.W. Anderson (1958) introduced a tight-binding model to study the dynamics of an electron moving in a random medium. His model is described by the Schrödinger equation on the three-dimensional lattice $\mathbb{Z}^3$

$$i\hbar\dot{\varphi}_j = E_j\varphi_j + \sum_{k\neq j} V_{jk}\varphi_k,$$

where $\hbar = 1$, φ_j is the wave function, E_j is a random and independent variable, and V_{jk} is the interaction matrix that may or may not contain stochastic variables. From the physical point of view E_j is the potential energy of a spin occupying site j and $\sum_{k \neq j} V_{jk}\varphi_k$ is the kinetic energy of the particle which, in the absence of magnetic field, is given by the Laplacian. Anderson showed that, at sufficiently strong disorder, the interferences can start to dominate the transport. In this case, the material becomes a semiconductor.

The localisation studied by P.W. Anderson is sometimes called *strong dynamic localisation*. Here we use the definition given by Hundertmark (2000). Consider for any localised initial condition φ the part of φ with energy in the interval $[a, b]$. A random Schrödinger operator has strong dynamic localisation with energy in $[a, b]$ if φ stays in compact regions for all times up to arbitrary small errors.

Spectral localisation. Under some mild physically reasonable conditions, a random Schrödinger operator has *spectral localisation* in an energy interval $[a, b]$ if the spectrum of the Hamiltonian is a pure point (see Hundertmark (2000) for more details).

Anderson's localisation was initially given a spectral interpretation: for nearest neighbour interactions and random potential the spectrum is pure point and the corresponding eigenstates are exponentially localised (see Ishii (1973), Kunz & Souillard (1980), Pastur (1980) for the one-dimensional case and Martinelli & Scoppola (1985) for the multi-dimensional case). Indeed strong dynamic localisation and spectral localisation are closely related. One can find in the literature that both are sometimes called Anderson's localisation. By the RAGE theorem (due to Ruelle, Amrein, Georcescu and Enss) strong dynamic localisation implies spectral localisation, but the converse is not true. Counter examples of (non-random) one-dimensional Schrödinger operators were constructed by del Rio, Jitomirskaya, Last, & Simon (1996).

Many experiments and numerical simulations on localisation were done by solid-state physicists. Borland (1963) examined the one-dimensional localisation problem from a probabilistic perspective, while Dean & Bacon (1963) performed numerical simulations on disordered chains of atoms of finite length and showed that eigenstate localisation is more pronounced at high frequencies than at low frequencies.

After P.W. Anderson was awarded the Nobel prize, localisation due to disorder became a very popular topic. Nowadays the notion of Anderson's localisation is not restricted to electrons but used for any type of waves. In the 1980s, localisation due to disorder was found relevant in the context of

classical waves in random media (see Anderson (1985), Maynard (1988) and John (1991)).

Disordered spring-mass elastic systems. Dyson (1953) and Schmidt (1957) studied the effects of disorder on the vibration frequencies of a one-dimensional spring-mass chain in the limit when the chain is infinitely long. Though they did not study the influence of disorder on the eigenvectors or on wave propagation, their results help to explain wave transmission in such systems. Eigenstate localisation and wave propagation in disordered chains were investigated by Matsuda & Ishii (1970) and by Ishii (1973). Their approach is based on the theorem by Furstenberg (1963), which states that each bay of a disordered periodic structure can be modelled with a random transfer matrix and, as a result, the entire structure can be modelled with a product of random matrices.

In this paper we study disordered flexural and mass-spring systems, in which we observe eigenstate localisation. Though it is due to disorder, this is not the localisation in the sense of Anderson (1958), who considered a formally different problem. Nevertheless there are some similarities, and in the literature Anderson's localisation is sometimes related to the localisation of the eigenvectors of a random matrix (see Trefethen & Embree (2005), Chapter 36). For consistency, we will include both types of localisation under the broad name of "generalised Anderson's localisation".

In the case of continuous disordered systems of infinite volume, the spectrum splits into discrete and continuous parts. In some cases the continuous parts may disappear. For example, it was proved by Gol'dsheid, Molchanov, & Pastur (1977) that for a one-dimensional continuous random Schrödinger operator with a random homogeneous potential the spectrum has only pure points. The exact location of the spectrum and the criterions for a given part in the spectrum to be a pure point or purely continuous were obtained by Kunz & Souillard (1980). The discrete part of the spectrum is a good candidate to find localised eigenstates. In the case of discrete systems, the spectrum has no continuous parts. However, as demonstrated by our simulations, the spectrum can be represented as the union of two parts by analogy with the continuous model. One part - where we observe eigenstate localisation - can be thought as the "discrete" part of the spectrum, while the other part - where points of the spectrum cluster - can be thought as the "continuous" part of the spectrum. Furthermore, in the case of a medium with a gap in the spectrum, Klein & Koines (2001) proved that the spectral gap shrinks (possibly closing) as randomness is added to the medium, and

localisation occurs at the edges of the gap.

1.3. The structure of the paper

The paper is organised as follows. In Section 2 we present the results for a bi-coupled system made of translational and rotational masses connected by non-inertial beams, both when the system is ordered and disordered. Then, we show that in some situations this system can be well approximated by simpler mono-coupled structures consisting of one (Section 3) or two (Section 4) types of point masses linked by springs. In Section 5 we analyse a more sophisticated bi-coupled system, made of two types of disks. Finally, in Section 6 we provide some concluding remarks.

2. Discrete bi-coupled system

We consider a system made of masses m_i with rotational inertia I_i, connected in series by Euler-Bernoulli beams of length l, flexural stiffness EJ and mass per unit length μ (see Fig. 3a). In the time-harmonic regime, the equation of motion of the beam is given by

$$\frac{\mathrm{d}^4 v(x)}{\mathrm{d}x^4} - \beta^4 v(x) = \left(\frac{\mathrm{d}^2}{\mathrm{d}x^2} + \beta^2\right)\left(\frac{\mathrm{d}^2}{\mathrm{d}x^2} - \beta^2\right) v(x) = 0, \tag{1}$$

where $v(x)$ is the transverse displacement, x is the spatial coordinate and $\beta = (\mu\omega^2/EJ)^{1/4}$, being ω the angular frequency. The solution of Eq. (1) can be written as the superposition of propagating waves of Helmholtz type (v_H) and decaying waves of modified Helmholtz type (v_M), namely

$$v(x) = v_H(x) + v_M(x), \tag{2}$$

where

$$\left(\frac{\mathrm{d}^2}{\mathrm{d}x^2} + \beta^2\right) v_H(x) = 0, \tag{3a}$$

$$\left(\frac{\mathrm{d}^2}{\mathrm{d}x^2} - \beta^2\right) v_M(x) = 0. \tag{3b}$$

For the system in Fig. 3a, the beam equation (1) needs to be complemented by the equations of linear and angular momentum balance of the concentrated mass.

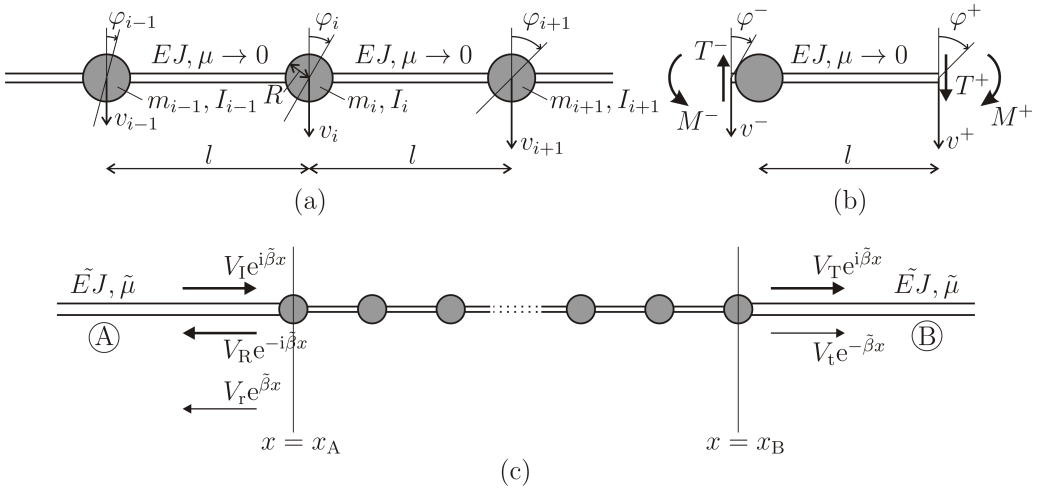

Figure 3: (a) Discrete bi-coupled system, consisting of translational and rotational masses connected by Euler-Bernoulli beams; (b) unit cell of the system; (c) transmission problem for the discrete flexural system, placed between two homogeneous semi-infinite Euler-Bernoulli beams with flexural stiffness $\tilde{EJ}$ and linear density $\tilde{\mu}$.

The transfer matrix $\mathbf{T}_i$ of a generic unit cell of the system, sketched in Fig. 3b, links the vector $\mathbf{U}^+$ of generalised displacements and forces at the end of the cell to the analogous vector $\mathbf{U}^-$ at the beginning of the cell:

$$\mathbf{U}^+ = \begin{Bmatrix} v^+ \\ \varphi^+ \\ T^+ \\ M^+ \end{Bmatrix} = \mathbf{T}_i \, \mathbf{U}^- = \begin{bmatrix} T^i_{11} & T^i_{12} & T^i_{13} & T^i_{14} \\ T^i_{21} & T^i_{22} & T^i_{23} & T^i_{24} \\ T^i_{31} & T^i_{32} & T^i_{33} & T^i_{34} \\ T^i_{41} & T^i_{42} & T^i_{43} & T^i_{44} \end{bmatrix} \begin{Bmatrix} v^- \\ \varphi^- \\ T^- \\ M^- \end{Bmatrix}. \tag{4}$$

Here $\varphi(x) = v'(x)$ is the rotation, $M(x) = EJv''(x)$ is the bending moment and $T(x) = -EJv'''(x)$ is the shear force. This system is bi-coupled since its motion is described by two kinematic variables: the transverse displacement $v(x)$ and the rotation $\varphi(x)$. The sign conventions for the kinematic and static variables of the problem are indicated in Fig. 3b. By imposing continuity conditions at the boundaries between the discrete mass and the beams, the following expression for the transfer matrix associated with the unit cell in

Fig. 3b is obtained:

$$\mathbf{T}_i = \begin{bmatrix} \frac{\cos(\beta l)+\cosh(\beta l)}{2} + & \frac{\sin(\beta l)+\sinh(\beta l)}{2\beta} + & \frac{\sin(\beta l)-\sinh(\beta l)}{2EJ\beta^3} & -\frac{\cos(\beta l)-\cosh(\beta l)}{2EJ\beta^2} \\ -\frac{m_i\omega^2[\sin(\beta l)-\sinh(\beta l)]}{2EJ\beta^3} & +\frac{I_i\omega^2[\cos(\beta l)-\cosh(\beta l)]}{2EJ\beta^2} & & \\ -\frac{\beta[\sin(\beta l)-\sinh(\beta l)]}{2} + & \frac{\cos(\beta l)+\cosh(\beta l)}{2} + & \frac{\cos(\beta l)-\cosh(\beta l)}{2EJ\beta^2} & \frac{\sin(\beta l)+\sinh(\beta l)}{2EJ\beta} \\ -\frac{m_i\omega^2[\cos(\beta l)-\cosh(\beta l)]}{2EJ\beta^2} & -\frac{I_i\omega^2[\sin(\beta l)+\sinh(\beta l)]}{2EJ\beta} & & \\ -\frac{EJ\beta^3[\sin(\beta l)+\sinh(\beta l)]}{2} + & \frac{EJ\beta^2[\cos(\beta l)-\cosh(\beta l)]}{2} + & \frac{\cos(\beta l)+\cosh(\beta l)}{2} & \frac{\beta[\sin(\beta l)-\sinh(\beta l)]}{2} \\ -\frac{m_i\omega^2[\cos(\beta l)+\cosh(\beta l)]}{2} & -\frac{I_i\omega^2\beta[\sin(\beta l)-\sinh(\beta l)]}{2} & & \\ -\frac{EJ\beta^2[\cos(\beta l)-\cosh(\beta l)]}{2} + & -\frac{EJ\beta[\sin(\beta l)-\sinh(\beta l)]}{2} + & -\frac{\sin(\beta l)+\sinh(\beta l)}{2\beta} & \frac{\cos(\beta l)+\cosh(\beta l)}{2} \\ +\frac{m_i\omega^2[\sin(\beta l)+\sinh(\beta l)]}{2\beta} & -\frac{I_i\omega^2[\cos(\beta l)+\cosh(\beta l)]}{2} & & \end{bmatrix}. \tag{5}$$

The transfer matrix is symplectic (Romeo & Luongo (2002); Yao, Zhong, & Lim (2009)), namely it satisfies the condition

$$\mathbf{T}_i^T \mathbf{\Omega} \mathbf{T}_i = \mathbf{\Omega}, \quad \text{where } \mathbf{\Omega} = \begin{bmatrix} \mathbf{0} & \mathbf{I}_2 \\ -\mathbf{I}_2 & \mathbf{0} \end{bmatrix}, \tag{6}$$

where $\mathbf{I}_2$ is the 2×2 identity matrix. Being symplectic, the transfer matrix has unit determinant and its first and third invariants coincide ($\mathcal{I}_1 = \mathrm{tr}(\mathbf{T}) = \mathcal{I}_3 = (\mathrm{tr}^3(\mathbf{T}) + 2\,\mathrm{tr}(\mathbf{T}^3) - 3\,\mathrm{tr}(\mathbf{T}^2)\,\mathrm{tr}(\mathbf{T}))/6$). Furthermore,

$$\mathbf{T}_i^{-1} = \begin{bmatrix} \mathbf{D}^T & -\mathbf{B}^T \\ -\mathbf{C}^T & \mathbf{A}^T \end{bmatrix} \quad \text{if } \mathbf{T}_i = \begin{bmatrix} \mathbf{A} & \mathbf{B} \\ \mathbf{C} & \mathbf{D} \end{bmatrix}, \tag{7}$$

where $\mathbf{A}$, $\mathbf{B}$, $\mathbf{C}$ and $\mathbf{D}$ are 2×2 matrices.

In the case of massless beams ($\mu \to 0$), the transverse displacement is a cubic function (see Eq. (1) for $\beta = 0$) and the transfer matrix admits this simplified form:

$$\mathbf{T}_i = \begin{bmatrix} \left(1 + \frac{m_i\omega^2 l^3}{6EJ}\right) & \left(l - \frac{I_i\omega^2 l^2}{2EJ}\right) & -\frac{l^3}{6EJ} & \frac{l^2}{2EJ} \\ \frac{m_i\omega^2 l^2}{2EJ} & \left(1 - \frac{I_i\omega^2 l}{EJ}\right) & -\frac{l^2}{2EJ} & \frac{l}{EJ} \\ -m_i\omega^2 & 0 & 1 & 0 \\ m_i\omega^2 l & -I_i\omega^2 & -l & 1 \end{bmatrix}. \tag{8}$$

The aim of this paper is to investigate the dynamic properties of discrete systems, hence we will assume that the beams are massless and that the total mass of the system is concentrated at the nodes of the beams. Accordingly, in the rest of the section we will compute the transfer matrix by means of Eq. (8).

2.1. Eigenvalue and transmission problems for the bi-coupled system

In this section, we formulate the two approaches considered in this paper: the eigenvalue problem and the transmission problem.

2.1.1. An auxiliary eigenvalue problem

The equations of linear and angular momentum balance of a generic mass i are given by

$$\frac{12EJ}{l^3}v_{i-1} + \frac{6EJ}{l^2}\varphi_{i-1} + \left(m_i\omega^2 - \frac{24EJ}{l^3}\right)v_i + \frac{12EJ}{l^3}v_{i+1} - \frac{6EJ}{l^2}\varphi_{i+1} = 0, \quad (9a)$$

$$-\frac{6EJ}{l^2}v_{i-1} - \frac{2EJ}{l}\varphi_{i-1} + \left(I_i\omega^2 - \frac{8EJ}{l}\right)\varphi_i + \frac{6EJ}{l^2}v_{i+1} - \frac{2EJ}{l}\varphi_{i+1} = 0. \quad (9b)$$

For a finite chain of n masses, the assembly of the equations of motion - complemented by the boundary conditions - leads to the classical eigenvalue problem

$$(\mathbf{A} - \lambda\mathbf{I})\,\mathbf{X} = \mathbf{0}, \quad \text{with } \mathbf{A} = \mathbf{M}^{-1}\mathbf{K}. \quad (10)$$

In the system above, $\mathbf{X} = \{v_1, \varphi_1, v_2, \varphi_2, \cdots, v_{n-1}, \varphi_{n-1}, v_n, \varphi_n\}^T$ is the vector of the unknowns, $\mathbf{M} = \mathrm{diag}\,(m_1, I_1, m_2, I_2, \cdots, m_{n-1}, I_{n-1}, m_n, I_n)$ is the mass matrix, $\lambda = \omega^2$ are the eigenvalues and $\mathbf{K}$ is the stiffness matrix. For a system with clamped ends, the stiffness matrix is obtained by imposing that the transverse displacements and the rotations at the ends are null: $v_0 = 0$,

$\varphi_0 = 0$, $v_{n+1} = 0$, $\varphi_{n+1} = 0$. In this case, the stiffness matrix is expressed by

$$\mathbf{K} = \begin{bmatrix}
\frac{24EJ}{l^3} & 0 & -\frac{12EJ}{l^3} & \frac{6EJ}{l^2} & 0 & & \cdots & & 0 \\
0 & \frac{8EJ}{l} & -\frac{6EJ}{l^2} & \frac{2EJ}{l} & 0 & & \cdots & & 0 \\
-\frac{12EJ}{l^3} & -\frac{6EJ}{l^2} & \frac{24EJ}{l^3} & 0 & -\frac{12EJ}{l^3} & \frac{6EJ}{l^2} & 0 & \cdots & 0 \\
\frac{6EJ}{l^2} & \frac{2EJ}{l} & 0 & \frac{8EJ}{l} & -\frac{6EJ}{l^2} & \frac{2EJ}{l} & 0 & \cdots & 0 \\
 & & & & \cdots & & & & \\
0 & \cdots & 0 & -\frac{12EJ}{l^3} & -\frac{6EJ}{l^2} & \frac{24EJ}{l^3} & 0 & -\frac{12EJ}{l^3} & \frac{6EJ}{l^2} \\
0 & \cdots & 0 & \frac{6EJ}{l^2} & \frac{2EJ}{l} & 0 & \frac{8EJ}{l} & -\frac{6EJ}{l^2} & \frac{2EJ}{l} \\
0 & \cdots & & 0 & -\frac{12EJ}{l^3} & -\frac{6EJ}{l^2} & \frac{24EJ}{l^3} & 0 & \\
0 & \cdots & & 0 & \frac{2EJ}{l} & 0 & \frac{8EJ}{l} & &
\end{bmatrix}. \quad (11)$$

If different boundary conditions are considered, the first two and the last two rows of matrix $\mathbf{K}$ need to be modified. In the example of Fig. 2 simply-supported boundary conditions were considered, namely the transverse displacements and the bending moments at the ends of the system were supposed to be zero.

The eigenvalues and eigenvectors of the discrete bi-coupled system are determined by solving Eq. (10). The square roots of the eigenvalues, $\omega = \sqrt{\lambda}$, represent the eigenfrequencies (or natural frequencies) of the system.

2.1.2. Transmission problem: energies and localisation factor

In order to better evaluate the transmission properties of the flexural system, we consider a finite stack of n masses that is connected to two homogeneous semi-infinite beams, indicated by A and B in Fig. 3c and having, for simplicity, the same flexural stiffness $\tilde{E}J$ and linear density $\tilde{\mu}$. We consider a right-travelling wave of amplitude $V_{\mathrm{I}} = 1$ propagating in beam A, which impinges on the discrete system at the left boundary. This incident wave is, generally, partly reflected by and partly transmitted through the discrete system. Consequently, in medium A the transverse displacement is given

by the superposition of the incident wave and of two reflected waves, one propagating to the left and one evanescent:

$$v_{\mathrm{A}}(x) = V_{\mathrm{I}}\mathrm{e}^{\mathrm{i}\tilde{\beta}x} + V_{\mathrm{R}}\mathrm{e}^{-\mathrm{i}\tilde{\beta}x} + V_{\mathrm{r}}\mathrm{e}^{\tilde{\beta}x}, \tag{12}$$

where $\tilde{\beta} = (\tilde{\mu}\omega^2/\tilde{E}J)^{1/4}$. In medium B the displacement field is the sum of two transmitted waves, one propagating to the right and the other one decaying exponentially:

$$v_{\mathrm{B}}(x) = V_{\mathrm{T}}\mathrm{e}^{\mathrm{i}\tilde{\beta}x} + V_{\mathrm{t}}\mathrm{e}^{-\tilde{\beta}x}. \tag{13}$$

The reflection and transmission coefficients V_{R}, V_{r} and V_{T}, V_{t} are obtained from the following system of equations (with $V_{\mathrm{I}} = 1$):

$$\begin{Bmatrix} v_{\mathrm{B}}(x=x_{\mathrm{B}}) \\ \varphi_{\mathrm{B}}(x=x_{\mathrm{B}}) \\ M_{\mathrm{B}}(x=x_{\mathrm{B}}) \\ T_{\mathrm{B}}(x=x_{\mathrm{B}}) \end{Bmatrix} = \begin{Bmatrix} \mathrm{e}^{\mathrm{i}\tilde{\beta}x_{\mathrm{B}}}V_{\mathrm{T}} + \mathrm{e}^{-\tilde{\beta}x_{\mathrm{B}}}V_{\mathrm{t}} \\ \mathrm{i}\tilde{\beta}\mathrm{e}^{\mathrm{i}\tilde{\beta}x_{\mathrm{B}}}V_{\mathrm{T}} - \tilde{\beta}\mathrm{e}^{-\tilde{\beta}x_{\mathrm{B}}}V_{\mathrm{t}} \\ \tilde{\beta}^2\tilde{E}J\mathrm{e}^{\mathrm{i}\tilde{\beta}x_{\mathrm{B}}}V_{\mathrm{T}} - \tilde{\beta}^2\tilde{E}J\mathrm{e}^{-\tilde{\beta}x_{\mathrm{B}}}V_{\mathrm{t}} \\ \mathrm{i}\tilde{\beta}^3\tilde{E}J\mathrm{e}^{\mathrm{i}\tilde{\beta}x_{\mathrm{B}}}V_{\mathrm{T}} + \tilde{\beta}^3\tilde{E}J\mathrm{e}^{-\tilde{\beta}x_{\mathrm{B}}}V_{\mathrm{t}} \end{Bmatrix} = \mathbf{T}^{(n)} \begin{Bmatrix} v_{\mathrm{A}}(x=x_{\mathrm{A}}) \\ \varphi_{\mathrm{A}}(x=x_{\mathrm{A}}) \\ M_{\mathrm{A}}(x=x_{\mathrm{A}}) \\ T_{\mathrm{A}}(x=x_{\mathrm{A}}) \end{Bmatrix}$$

$$= \begin{bmatrix} T_{11}^{(n)} & T_{12}^{(n)} & T_{13}^{(n)} & T_{14}^{(n)} \\ T_{21}^{(n)} & T_{22}^{(n)} & T_{23}^{(n)} & T_{24}^{(n)} \\ T_{31}^{(n)} & T_{32}^{(n)} & T_{33}^{(n)} & T_{34}^{(n)} \\ T_{41}^{(n)} & T_{42}^{(n)} & T_{43}^{(n)} & T_{44}^{(n)} \end{bmatrix} \begin{Bmatrix} \mathrm{e}^{\mathrm{i}\tilde{\beta}x_{\mathrm{A}}} + \mathrm{e}^{-\mathrm{i}\tilde{\beta}x_{\mathrm{A}}}V_{\mathrm{R}} + \mathrm{e}^{\tilde{\beta}x_{\mathrm{A}}}V_{\mathrm{r}} \\ \mathrm{i}\tilde{\beta}\mathrm{e}^{\mathrm{i}\tilde{\beta}x_{\mathrm{A}}} - \mathrm{i}\tilde{\beta}\mathrm{e}^{-\mathrm{i}\tilde{\beta}x_{\mathrm{A}}}V_{\mathrm{R}} + \tilde{\beta}\mathrm{e}^{\tilde{\beta}x_{\mathrm{A}}}V_{\mathrm{r}} \\ \tilde{\beta}^2\tilde{E}J\mathrm{e}^{\mathrm{i}\tilde{\beta}x_{\mathrm{A}}} + \tilde{\beta}^2\tilde{E}J\mathrm{e}^{-\mathrm{i}\tilde{\beta}x_{\mathrm{A}}}V_{\mathrm{R}} - \tilde{\beta}^2\tilde{E}J\mathrm{e}^{\tilde{\beta}x_{\mathrm{A}}}V_{\mathrm{r}} \\ \mathrm{i}\tilde{\beta}^3\tilde{E}J\mathrm{e}^{\mathrm{i}\tilde{\beta}x_{\mathrm{A}}} - \mathrm{i}\tilde{\beta}^3\tilde{E}J\mathrm{e}^{-\mathrm{i}\tilde{\beta}x_{\mathrm{A}}}V_{\mathrm{R}} - \tilde{\beta}^3\tilde{E}J\mathrm{e}^{\tilde{\beta}x_{\mathrm{A}}}V_{\mathrm{r}} \end{Bmatrix}, \tag{14}$$

where $\mathbf{T}^{(n)}$ is given by

$$\mathbf{T}^{(n)} = \prod_{i=1}^{n} \mathbf{T}_i. \tag{15}$$

The transfer matrices $\mathbf{T}_i$ in Eq. (15) can be all equal (ordered system) or different (disordered system). In the case of an ordered system, the matrices $\mathbf{T}_i$ are all the same and they can be expressed as

$$\mathbf{T}_i = \mathbf{T} = \mathbf{P}\boldsymbol{\Lambda}\mathbf{P}^{-1}, \tag{16}$$

where $\mathbf{P}$ and $\boldsymbol{\Lambda}$ are the matrices of eigenvectors and eigenvalues of $\mathbf{T}$, respectively. In this case, Eq. (15) is equivalent to

$$\mathbf{T}^{(n)} = \mathbf{P}\boldsymbol{\Lambda}^n\mathbf{P}^{-1}. \tag{17}$$

If the matrices $\mathbf{T}_i$ are different but coaxial, they can be written as

$$\mathbf{T}_i = \mathbf{P}\mathbf{\Lambda}_i\mathbf{P}^{-1}, \tag{18}$$

where the eigenvalue matrix $\mathbf{\Lambda}_i$ is different for different unit cells, while the eigenvector matrix $\mathbf{P}$ is the same for all cells. In this case, Eq. (15) is tantamount to

$$\mathbf{T}^{(n)} = \mathbf{P}\begin{bmatrix} \lambda_1^{(1)} \times \cdots \times \lambda_1^{(n)} & 0 & 0 & 0 \\ 0 & \lambda_2^{(1)} \times \cdots \times \lambda_2^{(n)} & 0 & 0 \\ 0 & 0 & \lambda_3^{(1)} \times \cdots \times \lambda_3^{(n)} & 0 \\ 0 & 0 & 0 & \lambda_4^{(1)} \times \cdots \times \lambda_4^{(n)} \end{bmatrix}\mathbf{P}^{-1}, \tag{19}$$

where the superscript of the eigenvalues in brackets indicates the number of the unit cell. In the case of a disordered system with non-coaxial matrices $\mathbf{T}_i$, Eq. (19) is not valid, therefore the more general formula (15) should be used to determine the transfer matrix of the whole system.

Neglecting the evanescent components, the reflected and transmitted energies are calculated as $\mathcal{R} = V_{\mathrm{R}}\overline{V_{\mathrm{R}}}$ and $\mathcal{T} = V_{\mathrm{T}}\overline{V_{\mathrm{T}}}$, where the bar stands for the complex conjugate. Obviously, the energy conservation law requires that $\mathcal{R} + \mathcal{T} = 1$. In the non-propagation ranges all the energy is reflected back, hence $\mathcal{R} \simeq 1$ and $\mathcal{T} \simeq 0$. For consistency, we assume that a propagation range is defined by the condition that the transmitted energy $\mathcal{T}$ is a very small quantity, more specifically $\mathcal{T} < 10^{-6}$. The widths of the propagation and non-propagation ranges depend on the size of the finite system. As the number of the unit cells is increased, the propagation ranges are reduced in extension. In the limit case of an infinite disordered mono-dimensional system, all states are localised.

The propagation characteristics of the bi-coupled system can be identified also by means of the localisation factor, which is by definition the smallest positive Lyapunov exponent (Castanier & Pierre (1995)) and is the inverse of the localisation length (Godin (2005)). The Lyapunov exponent is used to measure chaos in dynamic systems, as it represents the average rate of convergence (or divergence) between nearby trajectories in phase space; analogously, the localisation factor is used to measure the average rate of decay (or growth) of the wave amplitudes (Chen & Wang (2007)). For a bi-coupled system four Lyapunov exponents can be defined, two of which are positive and the other two are equal in absolute value but opposite in sign (due to the left-right symmetry of the propagation properties of the system).

The Lyapunov exponents are ordered as follows:

$$\gamma_1 \geq \gamma_2 \geq 0 \geq \gamma_3(=-\gamma_2) \geq \gamma_4(=-\gamma_1). \tag{20}$$

Thus, γ_2 is the localisation factor. In the propagation ranges $\gamma_2 \simeq 0$ ($\gamma_2 = 0$ in the limit case of an infinite system), since the wave propagates without attenuation; on the other hand, in the non-propagation ranges $\gamma_2 > 0$, the wave amplitude decays as $\mathrm{e}^{-\gamma_2}$ and the energy is attenuated as $\mathrm{e}^{-2\gamma_2}$ (Chen & Wang (2007)).

We determine the Lyapunov exponents by using the general formulation of the Wolf algorithm (Wolf, Swift, Swinney, & Vastano (1985)). First, we choose a set of four independent vectors, namely $v_{01}, \cdots, v_{04}$. These vectors are ortho-normalised by using the Gram-Schmidt Re-orthonormalisation (GSR) procedure; we indicate the orthonormalised vectors as $v'_{01}, \cdots, v'_{04}$. Then, we pre-multiply each vector v'_{0k} ($k = 1, \cdots, 4$) by the transfer matrix and we apply again the GSR procedure. These operations are repeated until the last unit cell of the system. The orthonormalised vectors computed up to the ith unit cell are indicated as v'_{ik}. Finally, each Lyapunov exponent is calculated as follows:

$$\gamma_k \simeq \frac{1}{n} \sum_{i=1}^{n} \ln\left(v_{ik} \cdot v'_{ik}\right) \quad k = 1, \cdots, 4\,, \tag{21}$$

where the dot indicates the scalar product. Formula (21) converges to the exact Lyapunov exponent as the number of cells n tends to infinity.

In the following, we assume that the discrete masses are disks of radius R and density (with dimensions of mass per unit area) ρ_i. The translational mass and the rotational inertia of each disk are given by $m_i = \pi R^2 \rho_i$ and $I_i = \pi R^4 \rho_i / 2$, respectively. First we study the case when the disks have the same density (ordered system), and then we consider the case when the density is perturbed randomly (disordered system).

2.2. Ordered system of disks

In an ordered (or perfect) system the density is the same for all disks, i.e. $\rho_i = \rho$ for $i = 1, \cdots, n$; accordingly, $m_i = m = \pi R^2 \rho$, $I_i = I = \pi R^4 \rho / 2$ and $\mathbf{T}_i = \mathbf{T}$.

If the system is periodic, namely if it consists of an infinite number of identical cells, we can impose Bloch-Floquet conditions at the ends of each

cell to obtain the dispersion relation, which is given in compact form by

$$\det\left(\mathbf{T} - \mathrm{e}^{\mathrm{i}kl}\mathbf{I}\right) = 0, \tag{22}$$

where k is the wave number, l is the distance between the disks and $\mathbf{I}$ is the identity matrix. Eq. (22) admits two positive solutions, which have the following explicit expressions:

$$\omega_{1,2} = \left(\frac{1}{mIl^4}\left\{2EJl\left[6I + 2ml^2 + (ml^2 - 6I)\cos(kl)\right]\right.\right.$$
$$\left.\left. \pm\sqrt{4EJ^2l^2\left[6I + 2ml^2 + (ml^2 - 6I)\cos(kl)\right]^2 - 192mIEJ^2l^4\sin^4\left(\frac{kl}{2}\right)}\right\}\right)^{1/2}. \tag{23}$$

The lower dispersion curve ω_1 and the upper dispersion curve ω_2 are hereafter referred to as *translational branch* and *rotational branch*, respectively. The reason is that the motion of the flexural system at frequencies belonging to the upper branch is characterised by small transverse displacements and large rotations, with this effect becoming more pronounced as the rotational inertia is decreased. At lower frequencies, transverse displacements increase in magnitude relatively to rotations; in particular, in the long-wave limit the motion is almost purely translational. In the limit case of a system with masses having negligible rotational inertia (e.g. in a system made of point masses), the upper dispersion curve diverges to infinity and the motion of the system - which is mainly translational - is described by the only lower dispersion curve. We prove the above statement by looking at the limits of the dispersion curves at the ends of the first Brillouin zone:

$$\omega_1(k = 0) = 0, \tag{24a}$$

$$\omega_1(k = \pi/l) = \sqrt{\frac{2EJl\left(ml^2 + 12I - |ml^2 - 12I|\right)}{mIl^4}}, \tag{24b}$$

$$\omega_2(k = 0) = 2\sqrt{\frac{3EJ}{Il}}, \tag{24c}$$

$$\omega_2(k = \pi/l) = \sqrt{\frac{2EJl\left(ml^2 + 12I + |ml^2 - 12I|\right)}{mIl^4}}. \tag{24d}$$

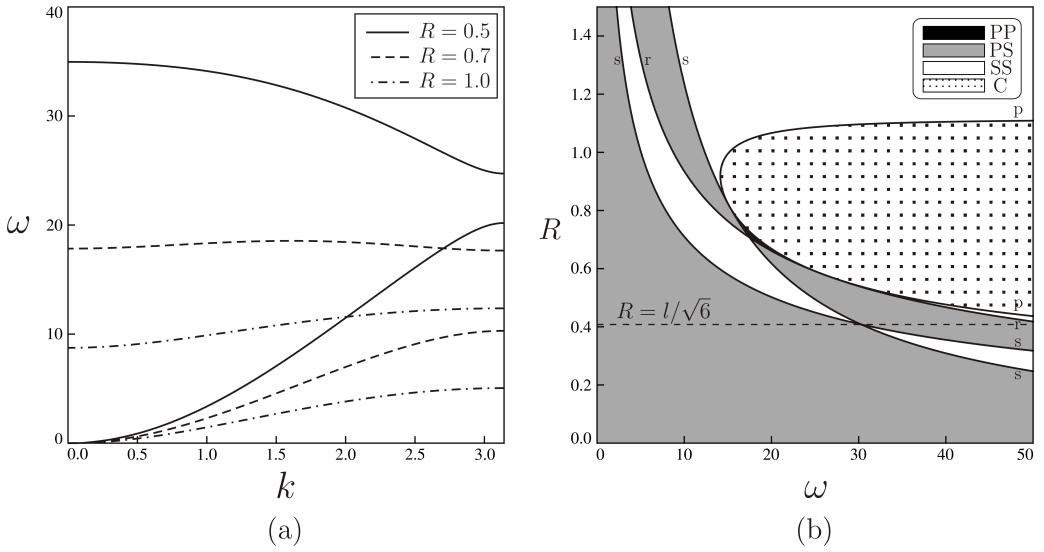

Figure 4: (a) Dispersion curves of the periodic disk-system for three different values of the disk radius; (b) representation of the propagation regions in the physical plane ω-R (for the calculations we have taken $\rho = 1$, $EJ = 10$, $l = 1$).

If the value of the translational mass m of the disks is kept constant while their rotational inertia I tends to zero, the limits above become:

$$\begin{aligned} &\lim_{I\to 0} \omega_1(k=0) = 0, \quad \lim_{I\to 0} \omega_1(k=\pi/l) = 4\sqrt{\frac{3EJ}{ml^3}}, \\ &\lim_{I\to 0} \omega_2(k=0) = \lim_{I\to 0} \omega_2(k=\pi/l) = \infty. \end{aligned} \tag{25}$$

Fig. 4a illustrates the dispersion curves obtained from three different values of the disk radius.

In bi-coupled periodic systems, four different propagation regions are distinguished (Romeo & Luongo (2002); Carta & Brun (2015)): the Pass-Pass (PP) zones, where two waves propagate with constant amplitude in each direction; the Pass-Stop (PS) zones, where one wave propagates and the other one is evanescent; the Stop-Stop (SS) zones, where both waves decay exponentially; and the Complex (C) zones, which are special SS Zones where the eigenvalues are complex conjugate and have moduli different from 1. These propagation regions are represented in the physical plane ω-R in Fig. 4b. The lines r, s and p, separating the different zones, are given respectively by

(Romeo & Luongo (2002); Carta & Brun (2015))

$$r:\ \mathcal{I}_2 = 2\,\mathcal{I}_1 - 2, \tag{26a}$$

$$s:\ \mathcal{I}_2 = -2\,\mathcal{I}_1 - 2, \tag{26b}$$

$$p:\ \mathcal{I}_2 = \frac{1}{4}\,\mathcal{I}_1^2 + 2. \tag{26c}$$

In the equations above, $\mathcal{I}_1$ and $\mathcal{I}_2$ are the first and second invariant of the transfer matrix:

$$\mathcal{I}_1 = \mathrm{tr}(\mathbf{T}) = \frac{24EJ + (ml^3 - 6Il)\omega^2}{6EJ}, \tag{27a}$$

$$\mathcal{I}_2 = \frac{1}{2}\left[\mathrm{tr}^2(\mathbf{T}) - \mathrm{tr}(\mathbf{T}^2)\right] = \frac{72EJ^2 - EJ(8ml^3 + 24Il)\omega^2 + mIl^4\omega^4}{12EJ^2}. \tag{27b}$$

For $R = l/\sqrt{6}$ the band-gap between the translational and rotational branches disappears, implying that for this value of the radius the two branches are connected.

In the following calculations we consider the particular case $R = 0.5$. The corresponding dispersion curves, drawn with solid lines in Fig. 4a, are reproduced in Fig. 5a with the normalised coordinates $\Omega = \omega\sqrt{ml^3/EJ}$ and kl. The limits of the bands are indicated by dashed lines.

In Fig. 5b we report the (normalised) eigenfrequencies of a finite disk-system with clamped ends, determined by means of Eqs. (10) and (11). The eigenfrequencies lie within the propagation bands of the corresponding periodic system, in accordance with the results of previous works (see, for instance, Mead (1975) and Brun, Giaccu, Movchan, & Movchan (2012)), apart from two eigenfrequencies which fall inside the band-gap between the two branches. However, the eigenvectors corresponding to the latter eigenfrequencies are extremely localised, as shown in the inset of Fig. 5b. Natural frequencies associated with localised eigenvectors and found inside the non-propagation zones have been observed also in other periodic bi-coupled systems (see Carta, Brun, & Movchan (2014a,b)). Localisation in ordered systems is influenced by boundary conditions. In the case of simply-supported boundary conditions, used in Fig. 2b, all the eigenfrequencies fall inside the propagation bands of the periodic system and the eigenvectors are not localised.

For the transmission problem, the reflected and transmitted energies are plotted in Figs. 5c and 5d, respectively. The energies are obtained by solving

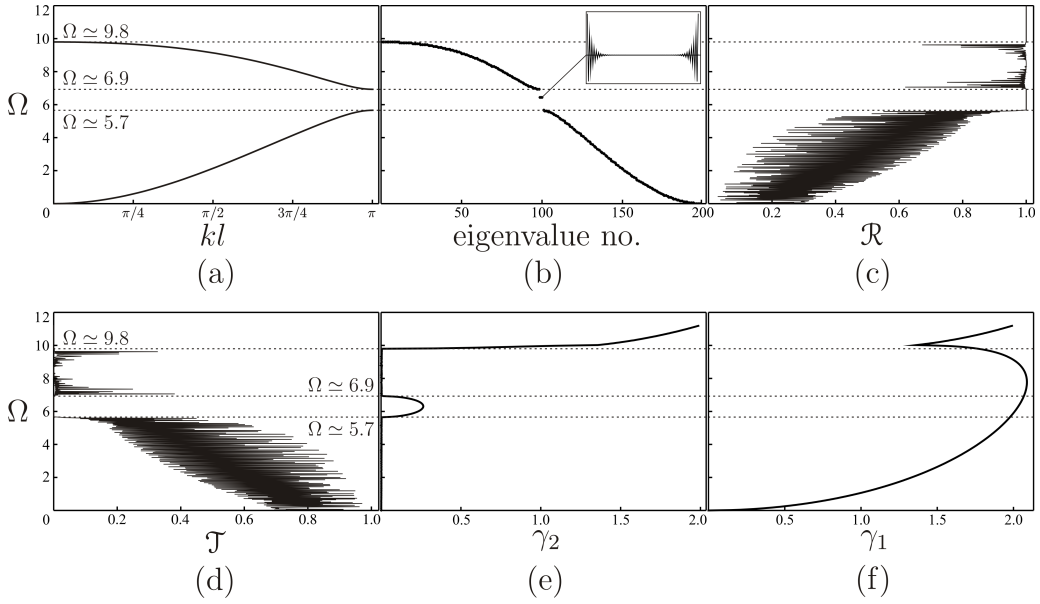

Figure 5: Dispersion curves for the periodic system of disks (a); eigenfrequencies (b), reflected energy (c), transmitted energy (d), localisation factor (e) and largest Lyapunov exponent (f) for the finite ordered system with $n = 100$ disks ($\rho = 1$, $R = 0.5$, $EJ = 10$, $l = 1$, $\tilde{EJ} = 1$, $\tilde{\mu} = 1$).

system (14) with $n = 100$. In correspondence of the dispersion curves of the periodic system, part of the energy is reflected back and part is transmitted through the disk-system (we have checked that $\mathcal{R} + \mathcal{T} = 1$ far from the boundaries between the disk-system and the homogeneous beams). On the contrary, in correspondence of the band-gaps of the periodic system almost all the energy coming from an external source is reflected back by the stack of disks, since $\mathcal{R} \simeq 1$ and $\mathcal{T} \simeq 0$.

In Figs. 5e and 5f we show the localisation factor γ_2 (i.e. the smallest positive Lyapunov exponent) and the largest Lyapunov exponent γ_1, respectively. $\gamma_2 \simeq 0$ in correspondence of the Pass-Stop zones of the periodic system and $\gamma_2 > 0$ in correspondence of the Stop-Stop zones. Conversely, γ_1 is positive for all frequencies, since in both directions one wave always decays exponentially.

2.3. Disordered system of disks

Now we assume that a parameter ζ of the system is perturbed with the variables ϵX_i ($\epsilon > 0$, $i = 1, \cdots, n$), where X_i are independent random variables with probability density functions f_i. Accordingly, the transfer matrix of the disordered system can be expressed as

$$\mathbf{T}_{\epsilon}^{(n)} = \prod_{i=1}^{n} \mathbf{T}_i^{\epsilon} = \prod_{i=1}^{n} \mathbf{T}_i(\zeta + \epsilon X_i). \tag{28}$$

We consider the case in which the random variables X_i have a *normal distribution* with zero mean value and unit variance:

$$f_i(x) = \frac{1}{\sigma\sqrt{2\pi}} \mathrm{e}^{-\frac{(x-\mu)^2}{2\sigma^2}}, \tag{29a}$$

$$< X_i >= \mu = \int x f_i(x) \mathrm{d}x = 0, \tag{29b}$$

$$\mathrm{var}(X_i) = \sigma^2 = \int x^2 f_i(x) \mathrm{d}x - < X_i >^2 = 1. \tag{29c}$$

In the following, we assume that the perturbed parameter of the system is the density ρ of the disks.

The eigenvalues and eigenvectors of a finite disordered system of n disks with clamped ends are computed by solving the eigenvalue problem (10), where in this case the mass matrix $\mathbf{M}$ contains random entries. The (normalised) eigenfrequencies calculated for $\epsilon = 0.1$ and for the average density

$\rho = 1$ are reported in Fig. 6a, where for comparison the limits of the propagation bands for the periodic system are indicated by dashed lines. The eigenfrequency intervals of the perturbed system are larger than those of the ordered system. This result is in accordance with the theory of *pseudospectra* (Trefethen & Embree (2005); Davies (2007)). The pseudospectrum of a square matrix $\mathbf{A}$ (as that in Eq. (10)) is defined as (Trefethen & Embree (2005))

$$\Lambda_\eta(\mathbf{A}) = \left\{ z \in \mathbb{C} : ||z\mathbf{I} - \mathbf{A}||^{-1} \geq \eta^{-1} \right\} \tag{30}$$

or, equivalently, as

$$\Lambda_\eta(\mathbf{A}) = \left\{ z \in \mathbb{C} : z \in \Lambda(\mathbf{A} + \Delta\mathbf{A}) \text{ for } ||\Delta\mathbf{A}|| < \eta \right\}, \tag{31}$$

for any $\eta \geq 0$. $\Lambda_\eta(\mathbf{A})$ is a larger set than the spectrum $\Lambda(\mathbf{A})$, even for very small values of η (Davies (2007)). This explains why the eigenvalue intervals of a disordered system are wider than those of the corresponding ordered system. Moreover, we notice the presence of isolated eigenfrequencies near the boundaries of the spectrum, in particular at high frequencies.

The eigenvectors calculated near the limits of the eigenfrequency ranges are localised, implying that at these frequencies the energy cannot be transmitted throughout the structure. For example, the eigenvector shown in Fig. 7a, which is associated with the largest eigenfrequency of the perturbed system, is highly localised near one end of the system. The largest eigenfrequency corresponding to an eigenvector that involves the whole structure (plotted in Fig. 7c) is found at $\Omega \simeq 8.9$. This value of Ω is smaller than the superior limit of the rotational branch $\Omega \simeq 9.8$ of the perfect periodic system (see Fig. 5). At $\Omega \simeq 9.8$ the eigenvector of the disordered system is very localised (Fig. 7b), meaning that this frequency belongs to the non-propagation region. Also at the inferior limit of the rotational branch, $\Omega \simeq 6.9$, and at the superior limit of the translational branch, $\Omega \simeq 5.5$, of the perfect periodic system, the eigenfrequencies of the perturbed structure are localised (see Figs. 7d and 7e). We can thus conclude that, though the eigenfrequency intervals of the disordered system are wider, the frequency ranges where waves can propagate in the perturbed structure are reduced with respect to the ordered system. It is interesting to observe that the major reductions occur at higher frequencies.

The results described above are confirmed by the diagrams in Figs. 6b, 6c and 6d, which show that $\mathcal{R} \simeq 1$, $\mathcal{T} \simeq 0$ and $\gamma_2 > 0$ in frequency intervals that are wider than the non-propagation regions of the ordered system.

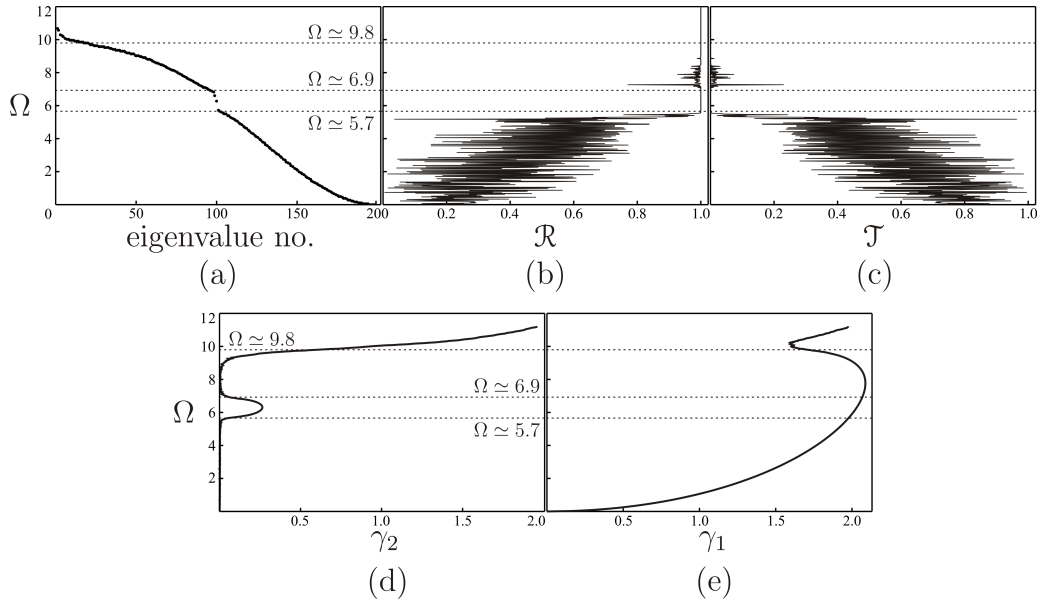

Figure 6: Eigenfrequencies (a), reflected energy (b), transmitted energy (c) and Lyapunov exponents (d,e) for a finite system of n disks with random density $\rho_i = \rho + \epsilon X_i$, where X_i have a normal distribution as in Eqs. (29) ($i = 1, \cdots, n$; $n = 100$; $\epsilon = 0.1$; $\rho = 1$; $R = 0.5$; $EJ = 10$; $l = 1$; $\tilde{EJ} = 1$; $\tilde{\mu} = 1$). The dashed lines are the limits of the Pass-Stop zones of the corresponding periodic system (see Fig. 5).

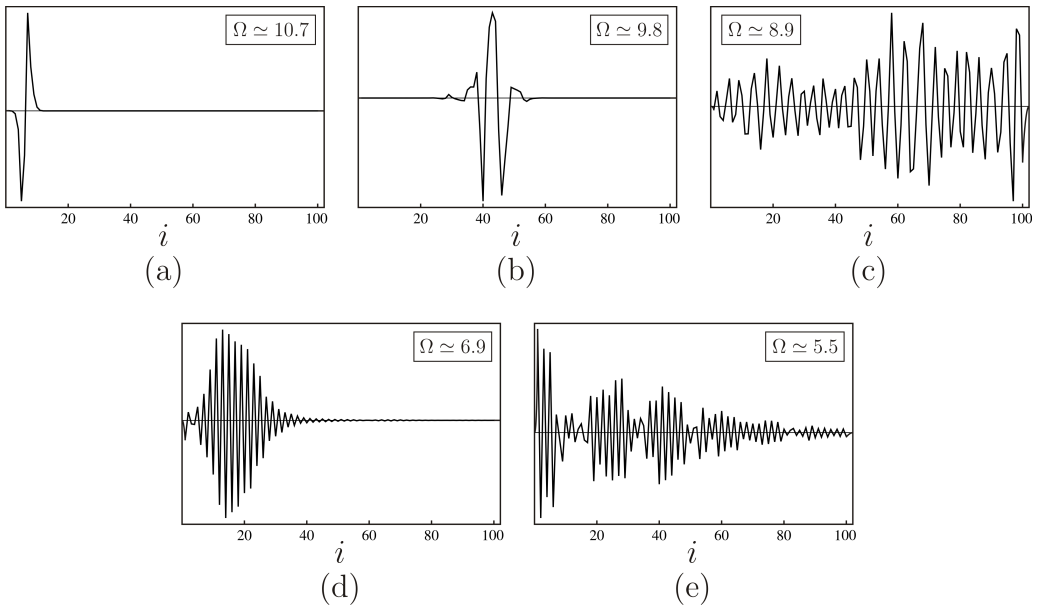

Figure 7: Eigenvectors of a finite disordered system of n disks associated with different (normalised) eigenfrequencies ($i = 1, \cdots, n$; $n = 100$; $\epsilon = 0.1$; $\rho = 1$; $R = 0.5$; $EJ = 10$; $l = 1$).

2.3.1. Random sub-systems inside an otherwise ordered disk-system

Here we consider the situation in which only one or two sub-systems of the structure are affected by random perturbations, while the rest is made of identical unit cells.

We start by examining the case of a system of $n = 100$ disks, where the density is the same everywhere except in the disks from 30 to 39. The (normalised) eigenfrequencies are plotted in Fig. 8a. Also when perturbation involves only a sub-system, the eigenfrequency range increases, mainly near the upper limit of the rotational branch. Moreover, in this case the eigenvectors corresponding to the eigenfrequencies falling in the non-propagation ranges are either localised within the random sub-system (see for instance Fig. 8b) or concern only the part of the system on the left or on the right of the random sub-interval (see for example Fig. 8c).

We also study the situation when two sub-systems have random density, in particular the sub-intervals made of disks 20-29 and 60-69. Generally, the eigenfrequency interval is larger when more units of the system are perturbed (compare Figs. 8a and 9a). Furthermore, most of the eigenvectors relative to

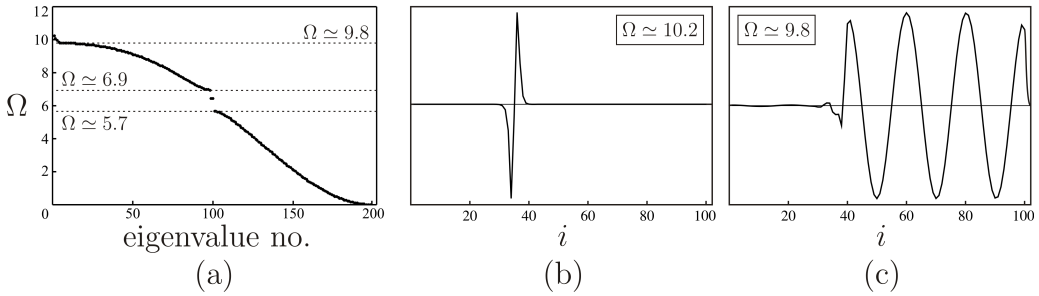

Figure 8: (a) Eigenfrequencies of a finite system of $n = 100$ disks, where $\rho_i = \rho$ for $i = 1, \cdots, 29$ and $i = 40, \cdots, 100$, while $\rho_i = \rho + \epsilon X_i$ for $i = 30, \cdots, 39$, with X_i having a normal distribution as in Eqs. (29); eigenvectors obtained at $\Omega \simeq 10.2$ (b) and $\Omega \simeq 9.8$ (c) ($\epsilon = 0.1$, $\rho = 1$, $R = 0.5$, $EJ = 10$, $l = 1$). The dashed lines in (a) are the limits of the Pass-Stop zones of the corresponding periodic system (see Fig. 5).

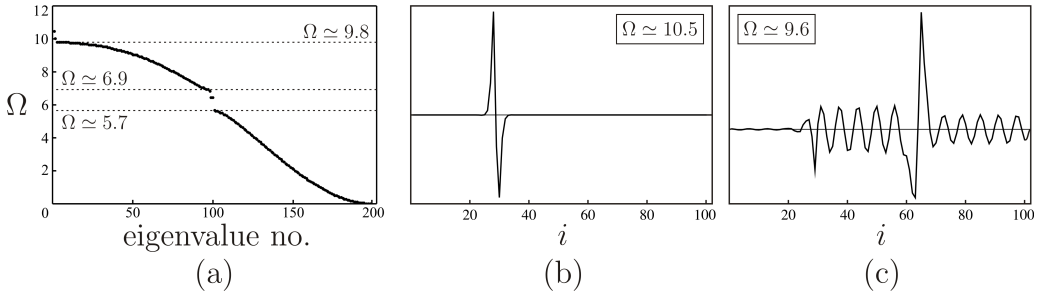

Figure 9: Eigenfrequencies (a) and two instances of eigenvectors (b,c) in the case of two perturbed sub-systems, i.e. $\rho_i = \rho + \epsilon X_i$ for $i = 20, \cdots, 29$ and $i = 60, \cdots, 69$, while $\rho_i = \rho$ elsewhere ($\epsilon = 0.1$, $\rho = 1$, $R = 0.5$, $EJ = 10$, $l = 1$). The dashed lines in (a) are the limits of the Pass-Stop zones of the corresponding periodic system (see Fig. 5).

the eigenfrequencies lying in the non-propagation ranges are different from zero either inside one of the two random sub-systems (see Figs. 9b and 9c) or in the ordered parts of the structure.

3. Discrete mono-coupled system

The time-harmonic equation of motion of a rod in absence of external forces is given by

$$EA\frac{\mathrm{d}^2u(x)}{\mathrm{d}x^2} + \rho A\omega^2 u(x) = 0, \tag{32}$$

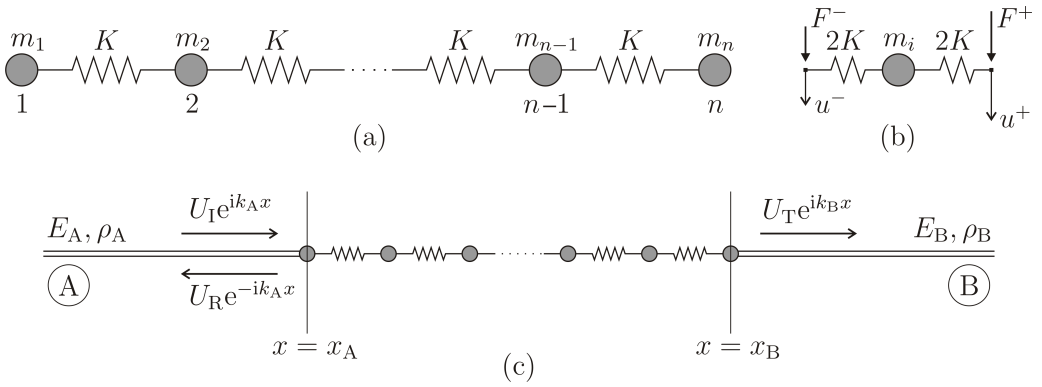

Figure 10: (a) Monatomic lattice consisting of n masses m_i linked by springs of uniform stiffness K; (b) unit cell of the system; (c) transmission problem for a monatomic lattice located between two semi-infinite elastic rods with elastic moduli $E_\mathrm{A}, E_\mathrm{B}$ and mass densities $\rho_\mathrm{A}, \rho_\mathrm{B}$.

where $u(x)$ is the displacement at the position x, E is the elastic modulus, ρ is the mass density, A is the cross-sectional area and ω is the angular frequency. If we assume that the total mass of the rod is lumped at points i separated by a distance l, Eq. (32) can be discretised as

$$\frac{EA}{l}\left(u_{i+1} - 2u_i + u_{i-1}\right) + m\omega^2 u_i = 0, \tag{33}$$

where $m = \rho A l$ is the concentrated mass at each point i. If this mass is not uniform and if we set $K = EA/l$, Eq. (33) takes the following form:

$$K\left(2u_i - u_{i-1} - u_{i+1}\right) - m_i\omega^2 u_i = 0. \tag{34}$$

Eq. (34) represents the equation of motion of a mass m_i $(i = 1, \cdots, n)$ of a chain of n particles connected by springs of stiffness K, which is illustrated in Fig. 10a. This system is known in the literature as *spring-mass system*, or *monatomic lattice* after Brillouin (1953), and it can be also used to model the dynamic response of continuous laminated structures in the low- and medium-frequency regimes (Carta & Brun (2012)).

The monatomic lattice is a mono-coupled system, because each mass has only one degree of freedom and the coupling between two adjacent cells is provided by the only force exerted by the spring. Consequently, in this case the transfer matrix is a 2×2 matrix and it relates the vector $\mathbf{u}^+$ of displacement and force at the end of each cell to the analogous vector $\mathbf{u}^-$ at the beginning of the cell:

$$\mathbf{u}^+ = \begin{Bmatrix} u^+ \\ F^+ \end{Bmatrix} = \mathbf{T}_i\, \mathbf{u}^- = \begin{bmatrix} T_{11}^i & T_{12}^i \\ T_{21}^i & T_{22}^i \end{bmatrix} \begin{Bmatrix} u^- \\ F^- \end{Bmatrix}. \tag{35}$$

The transfer matrix associated with the unit cell in Fig. 10b has the following expression:

$$\mathbf{T}_i = \begin{bmatrix} 1 - \frac{m_i\omega^2}{2K} & \frac{1}{K} - \frac{m_i\omega^2}{4K^2} \\ -m_i\omega^2 & 1 - \frac{m_i\omega^2}{2K} \end{bmatrix}. \tag{36}$$

3.1. Connection between the bi-coupled and mono-coupled systems

Eq. (32) is formally analogous to the Helmholtz equation (3a), which describes propagating waves in a continuous beam. This analogy is consistent only if the frequency parameter β in Eq. (3a) plays the role of the angular frequency ω or, more specifically, if β is substituted by $\sqrt{\rho/E}\,\omega$.

Similarly, in the discrete case the spring-mass system can be used to approximate the low-frequency behaviour of a bi-coupled system made of translational and rotational masses connected by non-inertial beams. To justify this claim, we consider a periodic monatomic lattice and assume that its unit cells are made of two masses m (see Fig. 11a). The total mass and moment of inertia of the two particles in the unit cell are given by $M = 2m$ and $I = ml^2/2 = Ml^2/4$, respectively. Indeed, the dispersion curve of the monatomic lattice approximates very well the translational branch of a bi-coupled discrete system with $I = Ml^2/4$ (see Fig. 11b), provided that the numerical value of the spring stiffness is chosen such that the slopes of the two curves in the long-wave limit are the same (i.e., $K = \sqrt{EJm/(2l^3)}$). Furthermore, it can be easily checked that the translational equation of motion (9a) of the bi-coupled discrete system can be expressed as the sum of the equations of motion (34) of the two particles in the unit cell of the monatomic lattice, supposing that the transverse displacement v and the rotation φ in Eq. (9a) are defined as the average of the displacement of the two particles and as the difference of the displacements of the two particles divided by their distance l, respectively.

If the rotational inertia I has a different value, it is preferable to employ a mono-coupled model with two different masses, m_1 and m_2, as also suggested by Kunin (1982). This model, which was named *biatomic lattice* by Brillouin (1953), is depicted in Fig. 12a for the case of an infinite number of identical cells. The total mass M and the total moment of inertia I with respect to the centroid G of particles m_1 and m_2 are $M = m_1 + m_2$ and $I = (m_1 m_2^2 + m_2 m_1^2) l^2/(m_1+m_2)^2$, respectively. If the values of M and I are given, masses

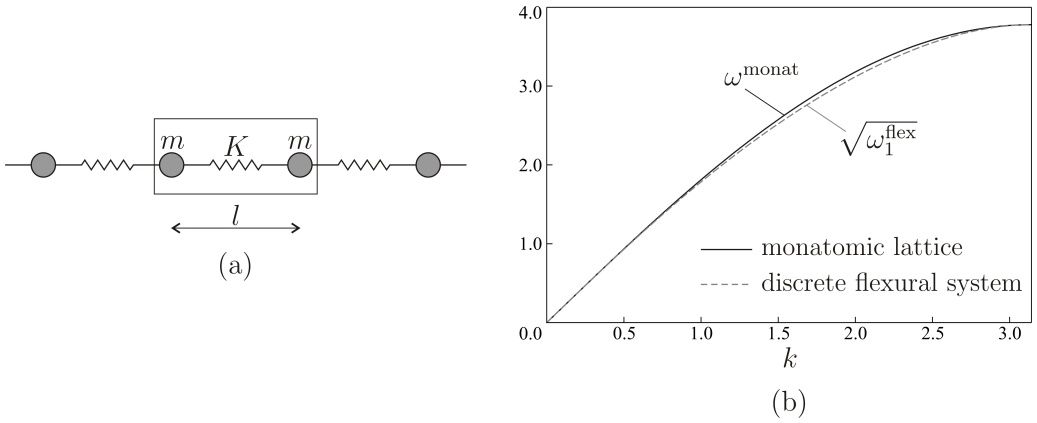

Figure 11: (a) Periodic monatomic lattice as an assembly of unit cells made of two particles; (b) comparison between the dispersion curve of the monatomic lattice (Eq. (50)) and the translational branch of a bi-coupled system with masses M having rotational inertia $I = Ml^2/4$ in terms of $\sqrt{\omega_1}$ (Eq. (23)) (the curves are drawn for $EJ = 10$, $l = 1$, $M = \pi/4$, $I = Ml^2/4$, $m = M/2$, $K = \sqrt{EJm/(2l^3)}$).

m_1 and m_2 can be derived from the following formula:

$$m_{1,2} = \frac{Ml \mp \sqrt{M^2l^2 - 4MI}}{2l}. \tag{37}$$

In Fig. 12b we compare the dispersion curves of the disk-system, examined in Section 2.2, and of the biatomic lattice, in which the spring stiffness is taken as $K = \sqrt{4EJM/l^3}$ to match the slopes of the curves at the origin. The figure shows that the lower branches of the two systems are very close to each other, while the upper branches are significantly different.

In order to improve the approximation at higher frequencies, we could choose the values of m_1 and m_2 such that the superior limits of the upper dispersion curves of the two systems be the same. Simple calculations lead to

$$m_{1,2} = \frac{M}{2} \mp \frac{1}{2}\sqrt{M^2 - \frac{8M\sqrt{3MI}}{\sqrt{3}l}}. \tag{38}$$

From the formula above it can be noticed that the superior limits of the upper branches of the two systems can coincide only if the value of the rotational inertia is limited from above, namely if $I < 3Ml^2/64$. If this is the case, both the lower and upper dispersion curves of the two systems are very close to

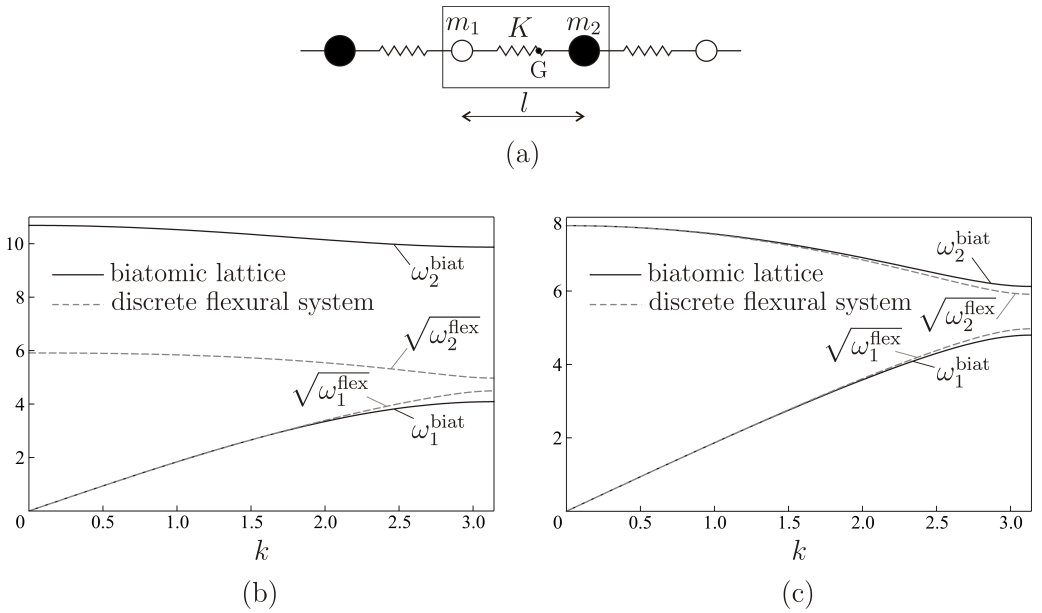

Figure 12: (a) Periodic biatomic lattice and identification of the unit cell; (b) branches $\sqrt{\omega_1}$ and $\sqrt{\omega_2}$ (Eq. (23)) of the disk-system analysed in Section 2.2 ($EJ = 10$, $l = 1$, $M = \pi/4$, $I = \pi/32$) and dispersion curves of the biatomic lattice (Eqs. (57)) with m_1 and m_2 given by Eq. (37) and $K = \sqrt{4EJM/l^3}$; (c) comparison of the dispersion curves $\sqrt{\omega_1}$ and $\sqrt{\omega_2}$ (Eq. (23)) of a bi-coupled flexural system ($EJ = 10$, $l = 1$, $M = \pi/4$, $I = \pi/96$) with the dispersion curves of the biatomic lattice (Eqs. (57)) with m_1 and m_2 determined from Eq. (38) and $K = \sqrt{4EJM/l^3}$.

each other (see Fig. 12c), hence the biatomic system can be used to model the more complex bi-coupled system examined in Section 2.2.

3.2. Eigenvalue and transmission problems for the mono-coupled system

3.2.1. Eigenvalue problem

We consider a finite lattice with free ends. The assembly of the equations of motion (34) leads to the following eigenvalue problem:

$$K \begin{bmatrix} 1 & -1 & & & \\ -1 & 2 & -1 & & \\ & \ddots & & & \\ & & -1 & 2 & -1 \\ & & & -1 & 1 \end{bmatrix} \begin{Bmatrix} u_1 \\ u_2 \\ \cdots \\ u_{n-1} \\ u_n \end{Bmatrix} - \omega^2 \begin{bmatrix} m_1 & & & & \\ & m_2 & & & \\ & & \ddots & & \\ & & & m_{n-1} & \\ & & & & m_n \end{bmatrix} \begin{Bmatrix} u_1 \\ u_2 \\ \cdots \\ u_{n-1} \\ u_n \end{Bmatrix} = \begin{Bmatrix} 0 \\ 0 \\ \cdots \\ 0 \\ 0 \end{Bmatrix}. \tag{39}$$

The first and last row of the stiffness matrix in Eq. (39) change if the lattice is subjected to different boundary conditions.

3.2.2. Transmission problem

The energies reflected by and transmitted through the monatomic lattice when a time-harmonic scalar wave of angular frequency ω impinges on it are determined by considering the discrete system to be perfectly connected to two semi-infinite elastic rods at its boundaries, labelled as A and B in Fig. 10c. The equation of motion of each rod j is given by

$$E_j \frac{\mathrm{d}^2 u_j(x)}{\mathrm{d}x^2} + \rho_j \omega^2 u_j(x) = 0 \quad j = \mathrm{A}, \mathrm{B}. \tag{40}$$

Here $E_\mathrm{A}, E_\mathrm{B}$ and $\rho_\mathrm{A}, \rho_\mathrm{B}$ are the elastic moduli and mass densities of the two rods, respectively. In addition, we denote as $c_\mathrm{A} = \sqrt{E_\mathrm{A}/\rho_\mathrm{A}}, c_\mathrm{B} = \sqrt{E_\mathrm{B}/\rho_\mathrm{B}}$ and $Q_\mathrm{A} = E_\mathrm{A}\omega/c_\mathrm{A}, Q_\mathrm{B} = E_\mathrm{B}\omega/c_\mathrm{B}$ the phase velocities and impedances of the two rods, respectively. In rod A the displacement field is represented by the sum of the incident and reflected waves:

$$u_\mathrm{A}(x) = U_\mathrm{I} \mathrm{e}^{\mathrm{i}k_\mathrm{A}x} + U_\mathrm{R} \mathrm{e}^{-\mathrm{i}k_\mathrm{A}x}, \tag{41}$$

where $k_\mathrm{A} = \omega/c_\mathrm{A}$ is the wave number. In rod B the displacement field has the form:

$$u_\mathrm{B}(x) = U_\mathrm{T} \mathrm{e}^{\mathrm{i}k_\mathrm{B}x}, \tag{42}$$

where $k_\mathrm{B} = \omega/c_\mathrm{B}$. Denoting the stresses in the rods by $\sigma_j = E_j \, \mathrm{d}u_j/\mathrm{d}x$ ($j = \mathrm{A}, \mathrm{B}$) and considering unit cross-sections, the following system of equations is derived:

$$\begin{aligned} &\begin{Bmatrix} u_\mathrm{B}(x = x_\mathrm{B}) \\ \sigma_\mathrm{B}(x = x_\mathrm{B}) \end{Bmatrix} = \begin{Bmatrix} U_\mathrm{T} \mathrm{e}^{\mathrm{i}k_\mathrm{B}x_\mathrm{B}} \\ \mathrm{i}k_\mathrm{B} E_\mathrm{B} U_\mathrm{T} \mathrm{e}^{\mathrm{i}k_\mathrm{B}x_\mathrm{B}} \end{Bmatrix} = \mathbf{T}^{(n)} \begin{Bmatrix} u_\mathrm{A}(x = x_\mathrm{A}) \\ \sigma_\mathrm{A}(x = x_\mathrm{A}) \end{Bmatrix} \\ &= \begin{bmatrix} T_{11}^{(n)} & T_{12}^{(n)} \\ T_{21}^{(n)} & T_{22}^{(n)} \end{bmatrix} \begin{Bmatrix} U_\mathrm{I} \mathrm{e}^{\mathrm{i}k_\mathrm{A}x_\mathrm{A}} + U_\mathrm{R} \mathrm{e}^{-\mathrm{i}k_\mathrm{A}x_\mathrm{A}} \\ \mathrm{i}k_\mathrm{A} E_\mathrm{A} \left(U_\mathrm{I} \mathrm{e}^{\mathrm{i}k_\mathrm{A}x_\mathrm{A}} - U_\mathrm{R} \mathrm{e}^{-\mathrm{i}k_\mathrm{A}x_\mathrm{A}} \right) \end{Bmatrix}. \end{aligned} \tag{43}$$

In this case, it is possible to write the expressions of the reflection and transmission coefficients, which are given by

$$\frac{U_\mathrm{R}}{U_\mathrm{I}} = \frac{Q_\mathrm{A} Q_\mathrm{B} T_{12}^n + T_{21}^n + \mathrm{i}\left(Q_\mathrm{A} T_{22}^n - Q_\mathrm{B} T_{11}^n\right)}{Q_\mathrm{A} Q_\mathrm{B} T_{12}^n - T_{21}^n + \mathrm{i}\left(Q_\mathrm{A} T_{22}^n + Q_\mathrm{B} T_{11}^n\right)} \mathrm{e}^{\mathrm{i}2k_\mathrm{A}x_\mathrm{A}} \tag{44}$$

and

$$\frac{U_{\mathrm{T}}}{U_{\mathrm{I}}} = \frac{\mathrm{i}2Q_{\mathrm{A}}}{Q_{\mathrm{A}}Q_{\mathrm{B}}T_{12}^n - T_{21}^n + \mathrm{i}\,(Q_{\mathrm{A}}T_{22}^n + Q_{\mathrm{B}}T_{11}^n)} \mathrm{e}^{\mathrm{i}(k_{\mathrm{A}}x_{\mathrm{A}} - k_{\mathrm{B}}x_{\mathrm{B}})}, \tag{45}$$

respectively. Accordingly, the reflected and transmitted energies are defined as

$$\mathcal{R} = \left|\frac{U_{\mathrm{R}}}{U_{\mathrm{I}}}\right|^2 = \frac{(Q_{\mathrm{A}}Q_{\mathrm{B}}T_{12}^n + T_{21}^n)^2 + (Q_{\mathrm{A}}T_{22}^n - Q_{\mathrm{B}}T_{11}^n)^2}{(Q_{\mathrm{A}}Q_{\mathrm{B}}T_{12}^n - T_{21}^n)^2 + (Q_{\mathrm{A}}T_{22}^n + Q_{\mathrm{B}}T_{11}^n)^2} \tag{46}$$

and

$$\mathcal{T} = \left|\frac{U_{\mathrm{T}}}{U_{\mathrm{I}}}\right|^2 \frac{Q_{\mathrm{B}}}{Q_{\mathrm{A}}} = \frac{4\,Q_{\mathrm{A}}Q_{\mathrm{B}}}{(Q_{\mathrm{A}}Q_{\mathrm{B}}T_{12}^n - T_{21}^n)^2 + (Q_{\mathrm{A}}T_{22}^n + Q_{\mathrm{B}}T_{11}^n)^2}. \tag{47}$$

Considering that $\det(\mathbf{T}^{(n)}) = 1$, it is easy to verify that $\mathcal{R} + \mathcal{T} = 1$, which represents the conservation of energy law. In the non-propagation ranges almost all the energy is reflected, therefore $\mathcal{R} \simeq 1$ and $\mathcal{T} \simeq 0$.

A mono-coupled system is characterised by two Lyapunov exponents, which are equal in absolute value but opposite in sign. The localisation factor is the positive Lyapunov exponent, which is defined as (Castanier & Pierre (1995))

$$\gamma = \lim_{n\to\infty} \frac{1}{n} \ln\left(\frac{\|\mathbf{u}_n\|}{\|\mathbf{u}_0\|}\right), \tag{48}$$

where $\mathbf{u}_n$ is the vector of displacement and force at the end of the nth cell, while $\mathbf{u}_0$ is the analogous vector at the beginning of the system. In the case of a finite number of cells, Eq. (48) can be approximated by (Castanier & Pierre (1995))

$$\gamma \simeq \frac{1}{n}\sum_{i=1}^{n} \ln\left|\left|\mathbf{T}_i \frac{\mathbf{u}_{i-1}}{\|\mathbf{u}_{i-1}\|}\right|\right|. \tag{49}$$

The formula above is equivalent to Eq. (21) for $k = 1$ (Castanier & Pierre (1995)). In the propagation ranges $\gamma \simeq 0$, since waves propagate without attenuation.

In Section 3.3 we assume that all masses are equal, while in Section 3.4 we perturb the masses randomly and evaluate the effects of the perturbation on the dynamic properties of the system.

3.3. Ordered monatomic system

Here we assume that $m_i = m$ and $\mathbf{T}_i = \mathbf{T}$ for $i = 1, \cdots, n$.

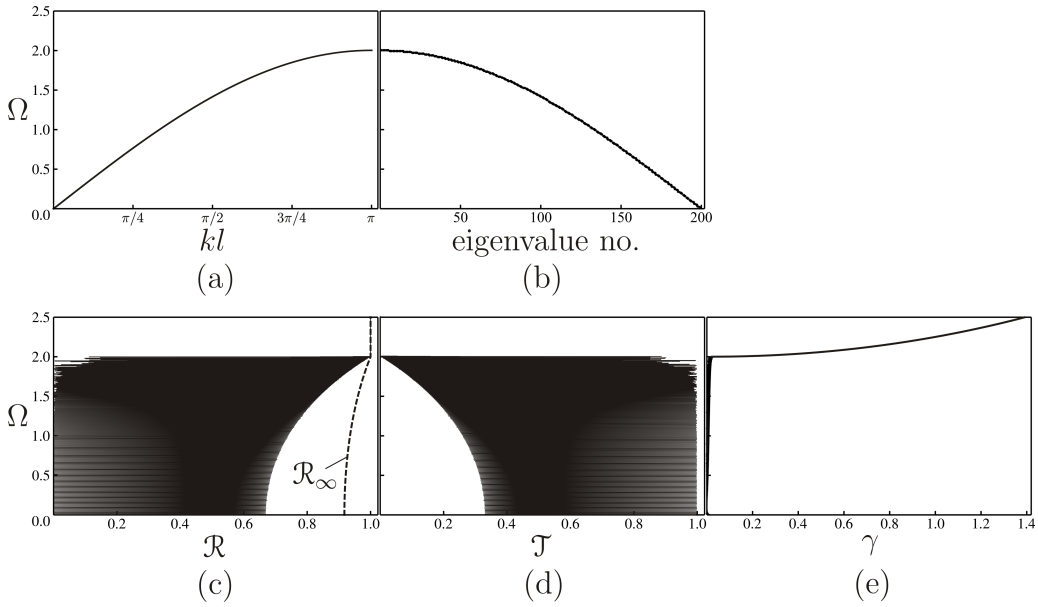

Figure 13: Dispersion curve (a) for the periodic monatomic lattice; eigenfrequencies (b), reflected energy (c), transmitted energy (d) and localisation factor (e) for the finite ordered monatomic lattice with $n = 200$ masses (for the calculations we have taken $m = 1$, $K = 10$, $E_{\mathrm{A}} = 1$, $c_{\mathrm{A}} = 1$, $E_{\mathrm{B}} = 1$, $c_{\mathrm{B}} = 1$).

The dispersion relation of the periodic system, which is obtained from Eq. (22) after introducing the expression (36) for the transfer matrix, has the explicit form

$$\omega = 2\sqrt{\frac{K}{m}}\left|\sin\left(\frac{kl}{2}\right)\right|, \tag{50}$$

where l is the distance between the masses and k is the wave number. The dispersion curve is shown in Fig. 13a, where $\Omega = \omega\sqrt{m/K}$ is the normalised frequency. For $\Omega < 2$ waves propagate without attenuation (pass-band), while for $\Omega > 2$ they decay exponentially (stop-band).

The eigenfrequencies of the finite lattice with $n = 200$ masses and free ends are computed by solving system (39). In this case, they can also be written in explicit form (see Lombardi & Rebaudo (1988)):

$$\omega_i = \sqrt{\frac{2K}{m}\left[1 - \cos\left(\frac{n-i}{n}\pi\right)\right]} \quad i = 1, \ldots, n. \tag{51}$$

By comparing Figs. 13a and 13b it can be seen that the eigenfrequencies of

the finite ordered lattice fall inside the pass-band of the periodic system. The corresponding eigenvectors are not localised. We observe that, if the ends of the system were fixed, two eigenfrequencies would lie in the band-gap, but their eigenvectors would be localised near the boundaries (similarly to what occurs in the flexural system with clamped ends, as shown in Fig. 5b).

In Figs. 13c, 13d and 13e we plot the reflected energy, the transmitted energy and the Lyapunov exponent as functions of the normalised frequency Ω. The dashed line in Fig. 13c represents the reflected energy for $n \to \infty$, which is given by (Felbacq, Guizal, & Zolla (1998))

$$\mathcal{R}_\infty = 1 - \frac{1 - \mathrm{tr}(\mathbf{T})^2/4}{\left(T_{12}Q_\mathrm{A} - T_{21}/Q_\mathrm{A}\right)^2} \quad \text{in the pass-band,} \tag{52a}$$

$$\mathcal{R}_\infty = 1 \quad \text{in the stop-band.} \tag{52b}$$

Fig. 13 shows that in the stop-band of the periodic system ($\Omega > 2$) $\mathcal{R} \simeq \mathcal{R}_\infty = 1$, $\mathcal{T} \simeq 0$ and $\gamma > 0$, while in the pass-band ($0 \leq \Omega \leq 2$) $\gamma \simeq 0$. We also point out that in the pass-band $|\mathrm{tr}(\mathbf{T})| \leq 2$, while in the stop-band $|\mathrm{tr}(\mathbf{T})| > 2$, as proved by Lekner (1994) and Felbacq et al. (1998).

3.4. Disordered monatomic system

Now we perturb the masses of the lattice by means of independent random variables ϵX_i, i.e. $m_i = m + \epsilon X_i$, where the variables X_i have a normal distribution with zero mean value and unit variance (see Eqs. (29)).

The reflected energy $\mathcal{R}$, the transmitted energy $\mathcal{T}$ and the localisation factor γ of the disordered lattice are plotted in Figs. 14a-14c, respectively, for $\epsilon = 0.1$ and $n = 200$. The comparison with the corresponding diagrams in Fig. 13 shows that the propagation range is reduced.

The eigenfrequencies of the finite lattice with free end masses are reported in Fig. 14d. By comparing Figs. 13b and 14d it can be seen that the range of eigenfrequencies of the perturbed array of masses is larger than that of the chain with equal masses. However, the eigenvectors calculated for the larger eigenfrequencies are localised, implying that energy cannot be transmitted at these frequencies. Some instances of localised eigenvectors are presented in Fig. 15. At $\Omega \simeq 2.09$ (Fig. 15a), which corresponds to the highest eigenfrequency, the wave is extremely localised. Energy localisation is reduced as lower values of the frequency are considered (Fig. 15b). The eigenvector calculated for $\Omega \simeq 1.83$, close to the highest frequency for which $\mathcal{T} \neq 0$, exhibits a pattern that is not clearly localised (Fig. 15c). In the

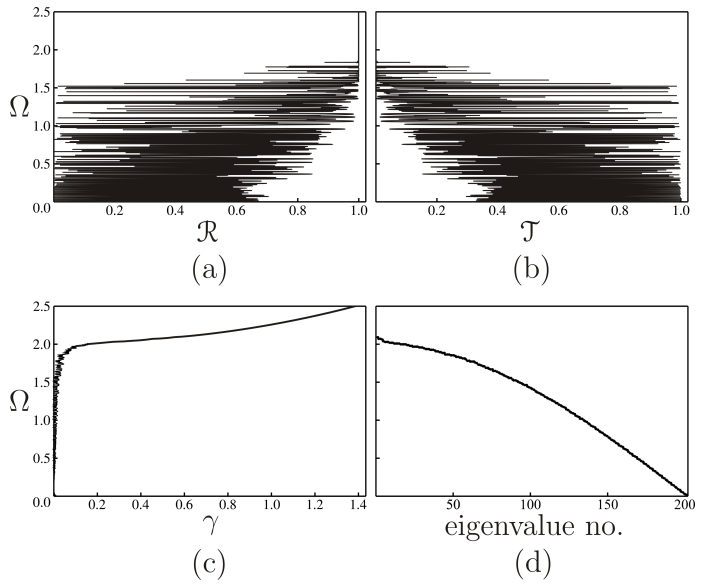

Figure 14: Reflected energy (a), transmitted energy (b), localisation factor (c) and eigenfrequencies (d) for the finite monatomic lattice with perturbed masses $m_i = m + \epsilon X_i$, where X_i have a normal distribution as in Eqs. (29) ($\epsilon = 0.1$, $n = 200$, $m = 1$, $K = 10$, $E_{\mathrm{A}} = 1$, $c_{\mathrm{A}} = 1$, $E_{\mathrm{B}} = 1$, $c_{\mathrm{B}} = 1$).

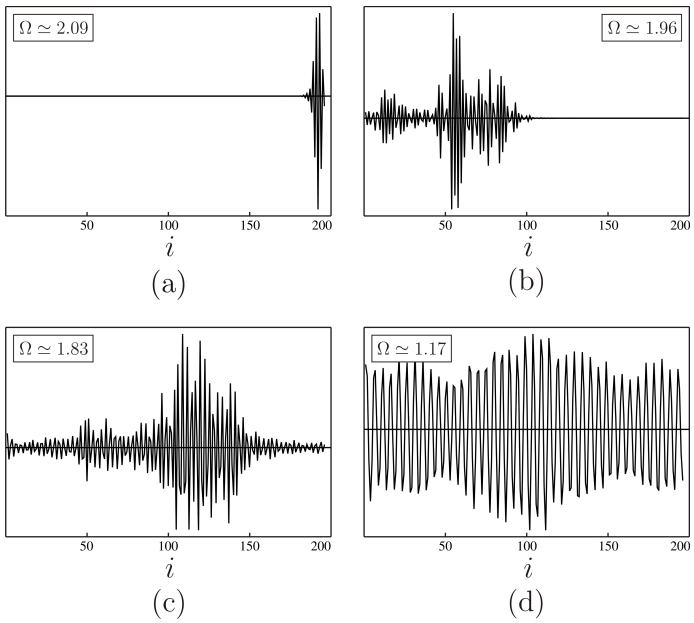

Figure 15: Eigenvectors of the finite perturbed monatomic lattice corresponding to different (normalised) eigenfrequencies ($i = 1, \cdots, n$; $n = 200$; $\epsilon = 0.1$; $m = 1$; $K = 10$).

propagation range non-localised eigenvectors are present, such as the one in Fig. 15d, though some slightly localised eigenvectors (due to the oscillation of the transmitted energy) can also be found.

The effect of localisation becomes more evident as the degree of disorder, represented by ϵ, increases. In Figs. 16a-16c we show the dependence of the transmitted energy on the normalised frequency Ω for $\epsilon = 0.05$, $\epsilon = 0.1$ and $\epsilon = 0.15$, respectively. The size of the propagation range decreases as ϵ is increased. We note peaks of transmission in the propagation range, while in the non-propagation range resonance modes are possible, but they are confined in an internal region of the mechanical system and energy cannot propagate from one boundary to the other.

The propagation range shortens also by increasing the number of masses n, as illustrated in Fig. 17. In particular, Figs. 17a, 17b and 17c show the transmitted energy $\mathcal{T}(\Omega)$ in a disordered lattice with $n = 50$, $n = 200$ and $n = 500$, respectively.

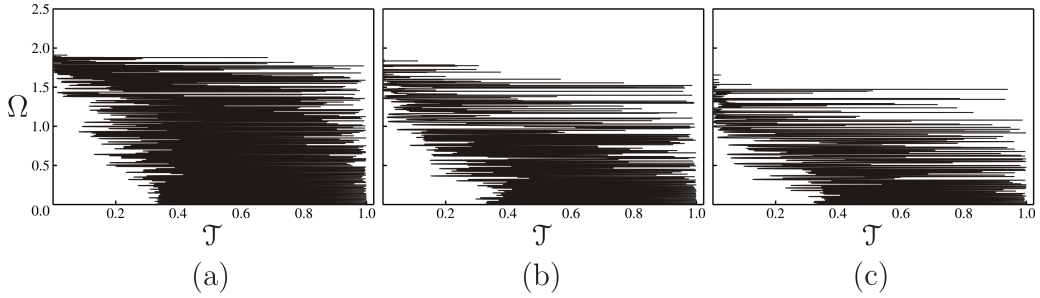

Figure 16: Transmitted energy in a finite perturbed monatomic lattice for $\epsilon = 0.05$ (a), $\epsilon = 0.1$ (b) and $\epsilon = 0.15$ (c) ($n = 200$, $m = 1$, $K = 10$).

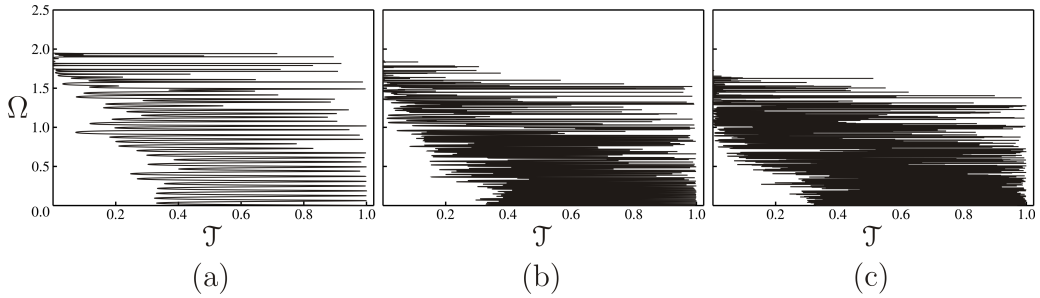

Figure 17: Transmitted energy in a finite perturbed monatomic lattice with $n = 50$ (a), $n = 200$ (b) and $n = 500$ (c) ($\epsilon = 0.1$, $m = 1$, $K = 10$).

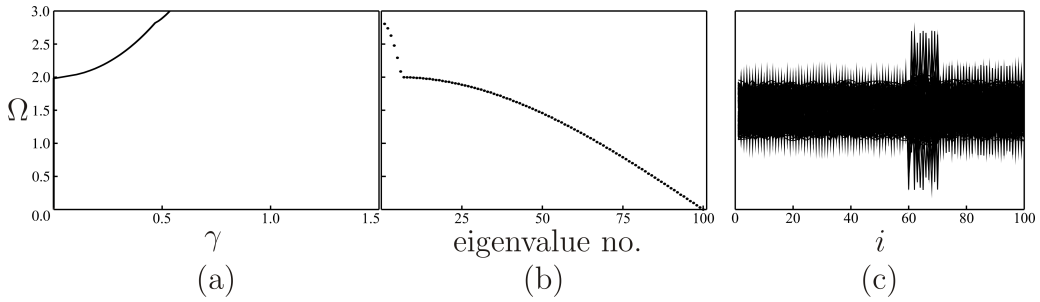

Figure 18: Lyapunov exponent (a), eigenfrequencies (b) and eigenvectors (c) for a monatomic lattice with $m_i = m$ for $i = 1, \cdots, 59$ and $i = 71, \cdots, 100$ and $m_i = m/2$ for $i = 60, \cdots, 70$ ($m = 1$, $K = 10$).

3.4.1. Random sub-systems inside an otherwise ordered lattice

In this section, we consider a finite ordered lattice in which one or two sub-systems have different masses.

Mass variation in one sub-system. First, we analyse a lattice with $n = 100$ masses, where $m_i = m$ for $i = 1, \cdots, 59$ and $i = 71, \cdots, 100$, while $m_i = m/2$ for $i = 60, \cdots, 70$. In Figs. 18a, 18b and 18c we plot, respectively, the Lyapunov exponent, the eigenfrequencies and all the eigenvectors of this system. By looking at Fig. 18b, we notice the appearance of localised eigenfrequencies for $\Omega > 2$ and that the eigenfrequency interval expands significantly with respect to the system with all masses equal (compare Figs. 18b and 13b), because the masses 60-70 are very different from the masses in the rest of the lattice. However, the frequency range where the Lyapunov exponent $\gamma \simeq 0$ is slightly shorter than in the case with all masses equal (compare Figs. 18a and 13e). The eigenvectors corresponding to the eigenfrequencies such that $\Omega > 2$ are localised in the sub-system 60-70, while the other eigenvectors are not localised (see Fig. 18c).

Now we assume that in the sub-interval 60-70 the masses take random values, i.e. $m_i = m + \epsilon X_i$ for $i = 60, \cdots, 70$, where X_i have a normal distribution as in Eqs. (29). In this case, the eigenfrequency range increases slightly with respect to the perfect system (compare Figs. 19b and 13b) and there are few localised eigenvectors (see Fig. 19c). Nonetheless, the Lyapunov exponent $\gamma > 0$ for $\Omega > 1.8$ (Fig. 19a), which implies that the propagation range of the system decreases significantly if the masses of a sub-system are assigned random values.

These two examples show that the introduction into an ordered system

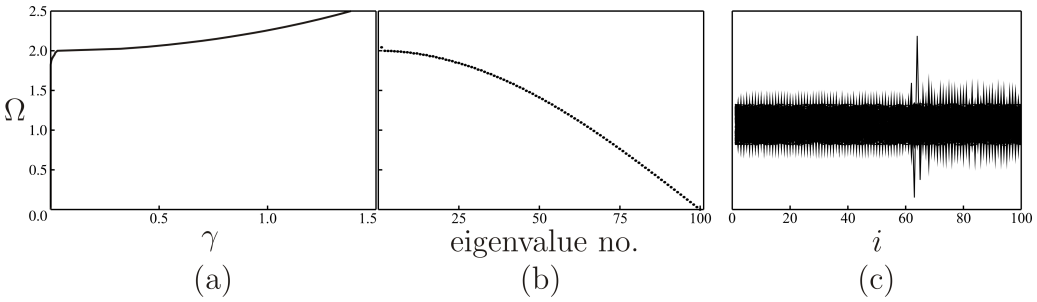

Figure 19: Lyapunov exponent (a), eigenfrequencies (b) and eigenvectors (c) for a monatomic lattice with $m_i = m$ for $i = 1, \cdots, 59$ and $i = 71, \cdots, 100$ and $m_i = m + \epsilon X_i$ for $i = 60, \cdots, 70$, with X_i given by Eqs. (29) ($\epsilon = 0.1$, $m = 1$, $K = 10$).

of a sub-region with strongly different but equal masses may change the eigenfrequencies of the system, but has a small effect on the widths of the propagation intervals. On the contrary, the propagation intervals are much more sensitive to randomness, since their widths are reduced even for small perturbations of the sub-system.

Cases with different distributions. We examine again the latter case of one random sub-system (made of masses 60-70), but considering different distributions for the random variables X_i. First, we assume that X_i have an *exponential distribution* with unit mean value and variance:

$$f_i(x) = \lambda \mathrm{e}^{-\lambda x}, \tag{53a}$$

$$< X_i >= \frac{1}{\lambda} = 1, \tag{53b}$$

$$\mathrm{var}(X_i) = \frac{1}{\lambda^2} = 1, \tag{53c}$$

where $f_i(x)$ are the probability density functions and where we have set $\lambda = 1$. The corresponding Lyapunov exponent, eigenfrequencies and eigenvectors are plotted in Fig. 20. With this distribution, the spectrum of the system expands dramatically and it exhibits localised eigenfrequencies for $\Omega > 2$ (Fig. 20b). On the other hand, the propagation range is reduced considerably (Fig. 20a). Localised eigenvectors are observed inside the random sub-interval also in this case (Fig. 20c).

Second, we consider the case in which the random variables X_i have a *Gamma distribution*, defined as

$$f_i(x) = \frac{x^{a-1}\mathrm{e}^{-x/b}}{b^a \Gamma(a)}, \tag{54a}$$

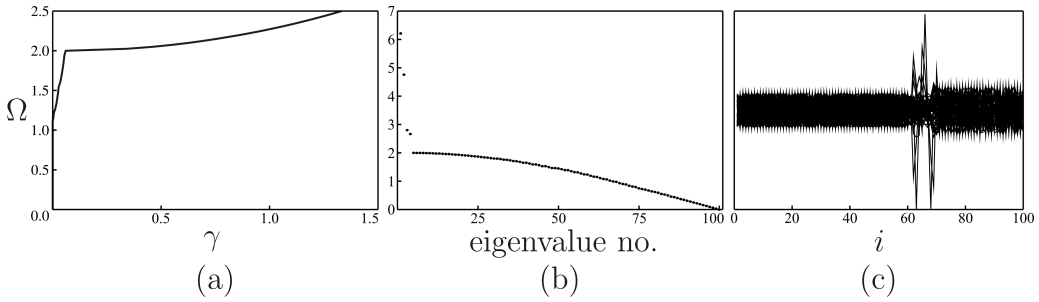

Figure 20: Results for a monatomic lattice with a random sub-system as in Fig. 19, but where the random variables X_i have an exponential distribution as in Eqs. (53) ($\lambda = 1$, $m = 1$, $K = 10$).

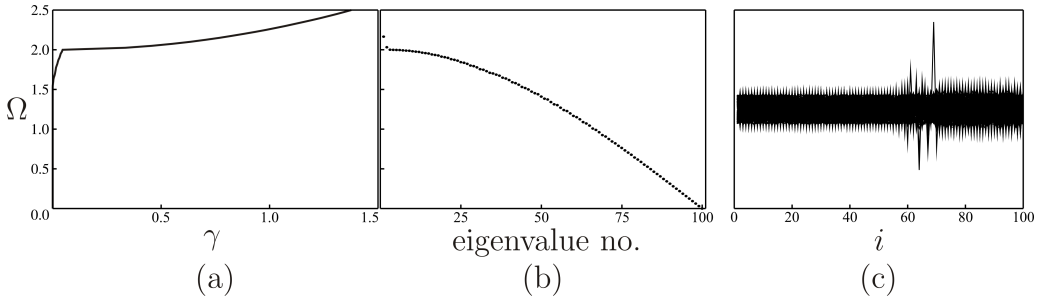

Figure 21: Results for a monatomic lattice with a random sub-system as in Fig. 19, but where the random variables X_i have a Gamma distribution as in Eqs. (54) ($a = 10$, $b = 0.1$, $m = 1$, $K = 10$).

$$< X_i >= a\, b = 1, \tag{54b}$$

$$\mathrm{var}(X_i) = a\, b^2 = 0.1, \tag{54c}$$

where $\Gamma(a)$ is the gamma function evaluated at a and where we have taken $a = 10$ and $b = 0.1$. The outcomes of the computations are shown in Fig. 21. Though only two eigenfrequencies are found for $\Omega > 2$ (Fig. 21b), the propagation range of the system decreases significantly since $\gamma > 0$ for $\Omega > 1.6$ (Fig. 21a).

Mass variation in two sub-systems. We study a monatomic lattice with two sub-systems having different masses from the rest of the structure, i.e. $m_i = m$ for $i = 1, \cdots, 9$, $i = 21, \cdots, 59$ and $i = 71, \cdots, 100$ and $m_i = m/2$ for $i = 10, \cdots, 20$ and $i = 60, \cdots, 70$. The results are reported in Fig. 22. For the sake of clarity, only the localised eigenvectors are plotted in Fig. 22c. The number of eigenfrequencies found for $\Omega > 2$ is the double of the

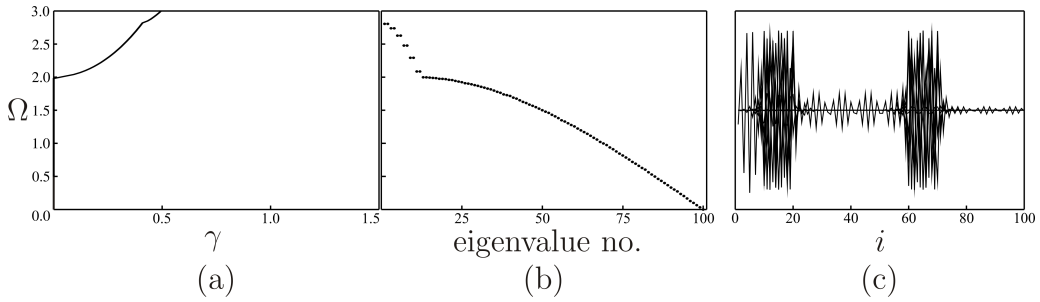

Figure 22: Lyapunov exponent (a), eigenfrequencies (b) and localised eigenvectors (c) for a monatomic lattice with $m_i = m$ for $i = 1, \cdots, 9$, $i = 21, \cdots, 59$ and $i = 71, \cdots, 100$ and $m_i = m/2$ for $i = 10, \cdots, 20$ and $i = 60, \cdots, 70$ ($m = 1$, $K = 10$).

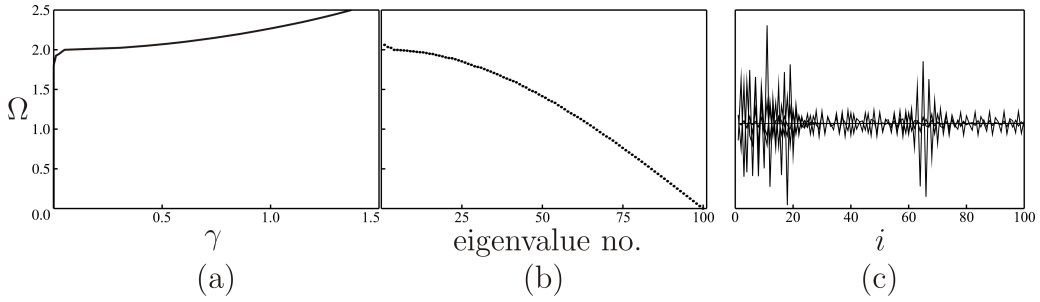

Figure 23: Lyapunov exponent (a), eigenfrequencies (b) and localised eigenvectors (c) for a monatomic lattice with $m_i = m$ for $i = 1, \cdots, 9$, $i = 21, \cdots, 59$ and $i = 71, \cdots, 100$ and $m_i = m + \epsilon X_i$ for $i = 10, \cdots, 20$ and $i = 60, \cdots, 70$, with X_i having a normal distribution as in Eqs. (29) ($\epsilon = 0.1$, $m = 1$, $K = 10$).

number of eigenfrequencies of the lattice with only one sub-system with half mass (see Fig. 18), but the upper limit of the eigenfrequency range does not change. The localised eigenvectors involve both sub-systems with half mass.

The outcomes for the case with two random sub-systems are illustrated in Fig. 23. By comparing Figs. 23 and 19, we can deduce that if the number of random sub-systems increases, generally the eigenfrequency range of the system is larger and the frequency interval for which waves propagate through the structure is smaller.

4. Discrete mono-coupled system with two types of masses

In Section 3.1 we showed that the translational and rotational branches of a bi-coupled discrete system made of masses M with rotational inertia I

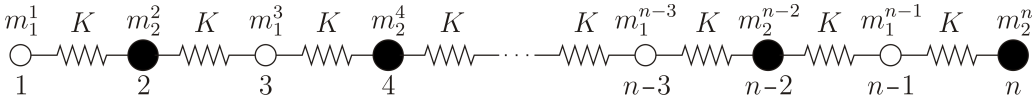

Figure 24: Biatomic lattice, made of two types of masses that can take random values.

are fitted very accurately by the dispersion curves of a biatomic lattice if $I < 3Ml^2/64$, where l is the distance between the masses. Therefore, it is of great interest to study the localisation and transmission properties of the biatomic lattice. In the following, we will discuss both the cases when the unit cells of the system are identical (Fig. 12a) and when the two masses have random values (Fig. 24).

The transfer matrix of a generic cell j is given by the product of the transfer matrices (36) of the two particles:

$$\mathbf{T}_j = \begin{bmatrix} 1 - \frac{m_2^{2j}\omega^2}{2K} & \frac{1}{K} - \frac{m_2^{2j}\omega^2}{4K^2} \\ -m_2^{2j}\omega^2 & 1 - \frac{m_2^{2j}\omega^2}{2K} \end{bmatrix} \begin{bmatrix} 1 - \frac{m_1^{2j-1}\omega^2}{2K} & \frac{1}{K} - \frac{m_1^{2j-1}\omega^2}{4K^2} \\ -m_1^{2j-1}\omega^2 & 1 - \frac{m_1^{2j-1}\omega^2}{2K} \end{bmatrix}. \tag{55}$$

The eigenvalues and eigenvectors of a finite system with n masses and free ends are determined by solving the following eigenvalue problem:

$$K \begin{bmatrix} 1 & -1 & & & \\ -1 & 2 & -1 & & \\ & \ddots & & & \\ & & -1 & 2 & -1 \\ & & & -1 & 1 \end{bmatrix} \begin{Bmatrix} u_1 \\ u_2 \\ \cdots \\ u_{n-1} \\ u_n \end{Bmatrix} - \omega^2 \begin{bmatrix} m_1^1 & & & & \\ & m_2^2 & & & \\ & & \ddots & & \\ & & & m_1^{n-1} & \\ & & & & m_2^n \end{bmatrix} \begin{Bmatrix} u_1 \\ u_2 \\ \cdots \\ u_{n-1} \\ u_n \end{Bmatrix} = \begin{Bmatrix} 0 \\ 0 \\ \cdots \\ 0 \\ 0 \end{Bmatrix}. \tag{56}$$

The reflected and transmitted energies and the localisation factor are computed from Eqs. (46), (47) and (49), respectively.

4.1. Ordered biatomic system

An ordered biatomic lattice consists of two masses that have the same values throughout the system, namely $m_1^i = m_1$ and $m_2^i = m_2$. Consequently, the transfer matrix is the same for all cells, i.e. $\mathbf{T}_j = \mathbf{T}$ for $j = 1, \cdots, n/2$.

The dispersion curves of the periodic biatomic lattice are obtained from Eq. (22). Their expressions can be written explicitly as

$$\omega_1 = \sqrt{\frac{K}{m_1 m_2}\left[(m_1+m_2) - \sqrt{(m_1+m_2)^2 - 4m_1m_2\sin\left(\frac{kl}{2}\right)^2}\right]} \tag{57a}$$

(*acoustic branch*) and

$$\omega_2 = \sqrt{\frac{K}{m_1 m_2}\left[(m_1+m_2)+\sqrt{(m_1+m_2)^2-4m_1m_2\sin\left(\frac{kl}{2}\right)^2}\right]} \qquad (57b)$$

(*optical branch*), where l is the distance between the particles and k is the wave number. Eqs. (57) are plotted in Fig. 25a in the normalised coordinates $\Omega = \omega\sqrt{m_1/K}$ and kl. The superior limit of the acoustic branch is given by $\omega = \sqrt{2K/m_2}$, while the inferior and the superior limits of the optical branch are $\omega = \sqrt{2K/m_1}$ and $\omega = \sqrt{2K(m_1+m_2)/(m_1m_2)}$ respectively.

Fig. 25b contains the (normalised) eigenfrequencies of the finite lattice with free ends, which are calculated from system (56). By comparing Fig. 25b with Fig. 25a we can see that the eigenfrequencies of the finite system lie within the pass-bands of the corresponding periodic system, as expected. Furthermore, all the eigenvectors are not localised.

For the transmission problem, Figs. 25c, 25d and 25e show how the reflected energy $\mathcal{R}$, the transmitted energy $\mathcal{T}$ and the localisation factor γ change with the normalised frequency Ω. The dashed line in Fig. 25c represents the reflected energy as $n \to \infty$, which is calculated by using Eqs. (52). Obviously, in correspondence of the stop-bands of the periodic system ($1 < \Omega < \sqrt{2}$ and $\Omega > \sqrt{3}$) $\mathcal{R} \simeq \mathcal{R}_\infty = 1$, $\mathcal{T} \simeq 0$ and $\gamma > 0$.

4.2. Disordered biatomic system

We start by perturbing only the larger masses m_2 with the random variables ϵX_j ($j = 1, \cdots, n/2$), i.e. $m_2^{2j} = m_2 + \epsilon X_j$ and $m_1^{2j-1} = m_1$. We assign to X_j the statistical properties defined by Eqs. (29).

Figs. 26a-26c illustrate how the reflected energy, the transmitted energy and the localisation factor vary with the normalised frequency $\Omega = \omega\sqrt{m_1/K}$, respectively. The upper limits of the optical and acoustic propagation ranges decrease with respect to the ordered system (see Fig. 25), while the lower limit of the optical propagation range remains unchanged. The reason is that the inferior limit of the optical pass-band of the corresponding periodic system is independent of m_2. Therefore, the effect of making m_2 vary randomly while keeping m_1 fixed is to reduce the propagation ranges from above.

Fig. 26d includes the eigenfrequencies of the perturbed system with free ends. The comparison between Figs. 25b and 26d shows that the eigenfrequency intervals of the perturbed system are larger than those of the ordered

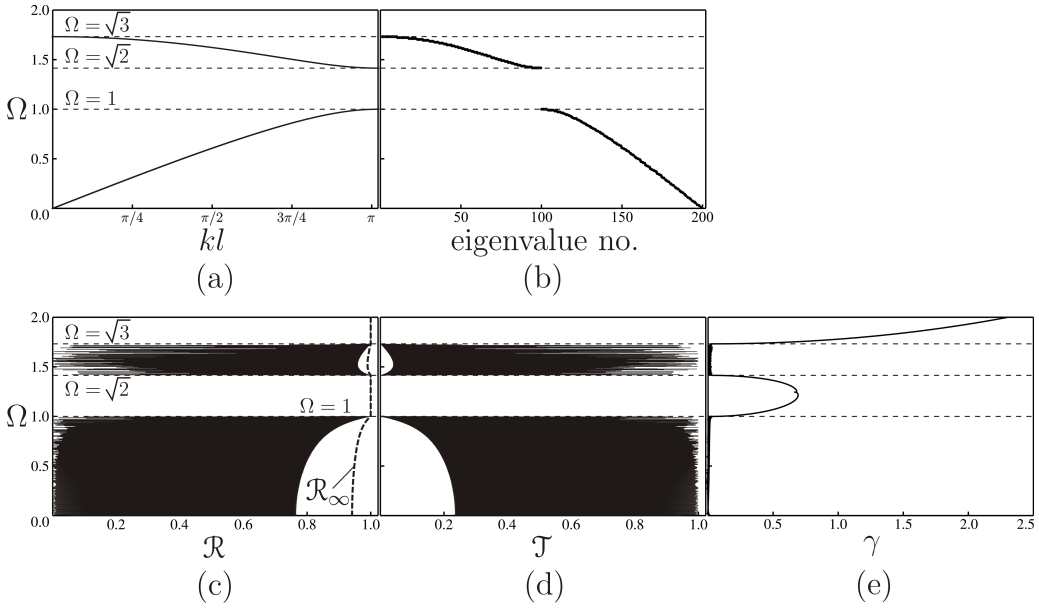

Figure 25: Acoustic and optical branches (a) for a periodic biatomic lattice; eigenfrequencies (b), reflected energy (c), transmitted energy (d) and localisation factor (e) for a finite ordered biatomic lattice with $n = 200$ masses ($m_1 = 1$, $m_2 = 2$, $K = 10$, $E_{\mathrm{A}} = 1$, $c_{\mathrm{A}} = 1$, $E_{\mathrm{B}} = 1$, $c_{\mathrm{B}} = 1$).

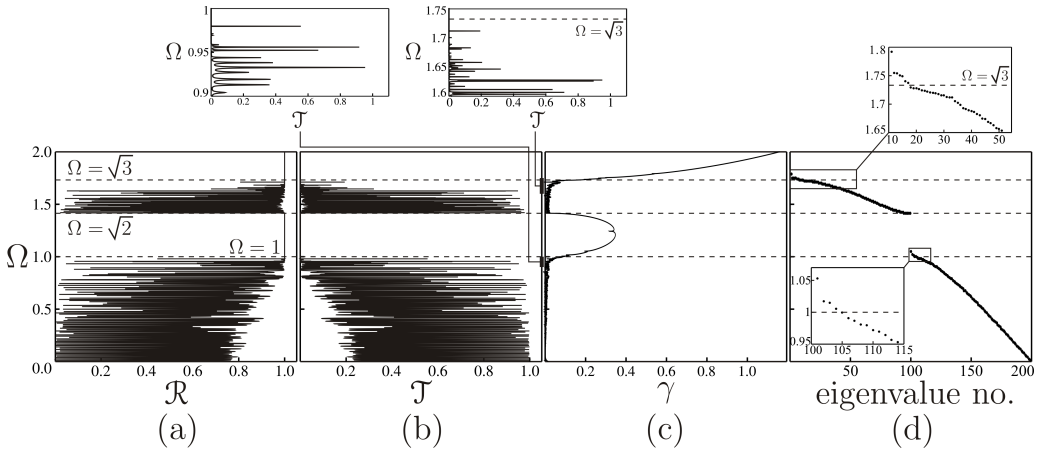

Figure 26: Reflected energy (a), transmitted energy (b), localisation factor (c) and eigenfrequencies (d) for a finite biatomic lattice after perturbing the masses m_2 with the independent random variables ϵX_j, with the properties specified in Eqs. (29) ($j = 1, \cdots, n/2$; $n = 200$; $\epsilon = 0.2$; $m_2 = 2$; $m_1 = 1$; $K = 10$; $E_{\mathrm{A}} = 1$; $c_{\mathrm{A}} = 1$; $E_{\mathrm{B}} = 1$; $c_{\mathrm{B}} = 1$). The dashed lines indicate the limits of the pass-bands of the periodic system.

system. However, the eigenfrequencies of the perturbed system near the upper limits of the two intervals are associated with localised modes. Other localised modes appear to arise at frequencies inside the propagation ranges, as observed also for the monatomic lattice discussed in Section 3.

Next, we consider the situation in which we keep m_2 fixed and make m_1 vary randomly, namely $m_1^{2j-1} = m_1 + \epsilon X_j$ and $m_2^{2j} = m_2$ ($j = 1, \cdots, n/2$). The results obtained for $\epsilon = 0.1$ are reported in Fig. 27, which shows that the optical propagation range is reduced significantly, while the acoustic propagation range is not modified with respect to the unperturbed case. This is explained by noting that the limits of the optical branch of the corresponding periodic system depend on the perturbed quantity m_1, while the superior limit of the acoustic branch does not.

Finally, we assume that both m_1 and m_2 vary randomly and independently from each other: $m_1^i = m_1 + \epsilon X_i$, $m_2^i = m_2 + \epsilon X_i$ ($i = 1, \cdots, n$). In this case, the optical propagation range almost disappears and the acoustic propagation range slightly shrinks, as illustrated in Fig. 28. This is a further indication that the effects of random perturbations are more significant at higher frequencies. Similar results are found if the spring stiffness K is varied randomly and the other parameters are uniform throughout the system.

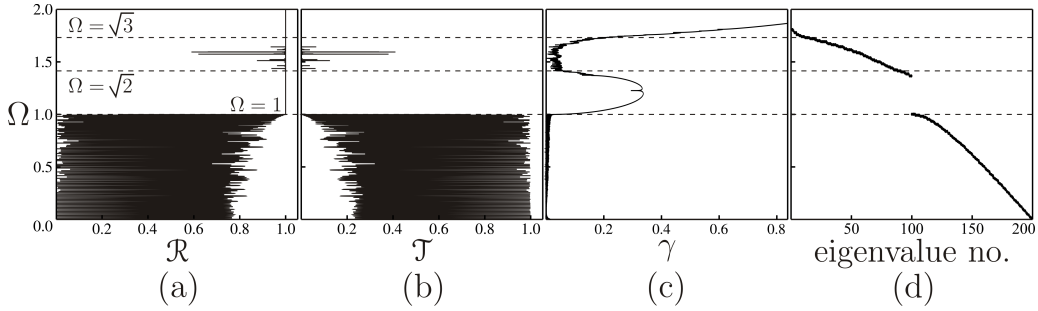

Figure 27: Reflected energy (a), transmitted energy (b), localisation factor (c) and eigenfrequencies (d) for a finite biatomic lattice with $m_1^{2j-1} = m_1 + \epsilon X_j$ and $m_2^{2j} = m_2$ ($j = 1, \cdots, n/2$; $n = 200$; $\epsilon = 0.1$; $m_1 = 1$; $m_2 = 2$; $K = 10$; $E_{\rm A} = 1$; $c_{\rm A} = 1$; $E_{\rm B} = 1$; $c_{\rm B} = 1$). The dashed lines indicate the limits of the pass-bands of the periodic system.

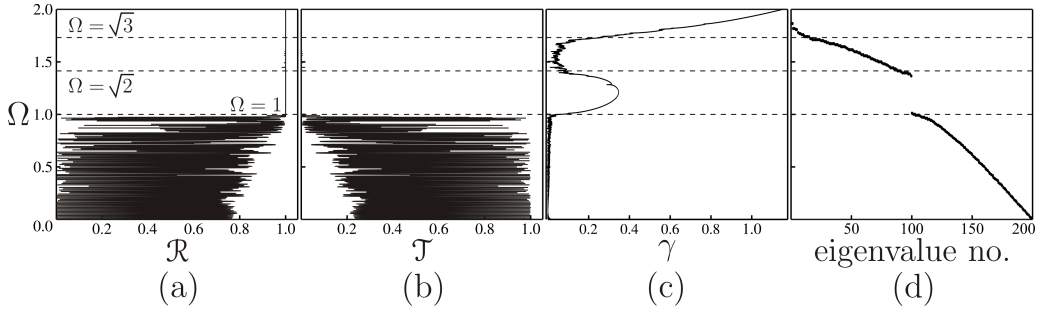

Figure 28: Reflected energy (a), transmitted energy (b), localisation factor (c) and eigenfrequencies (d) for a finite biatomic lattice with $m_1^i = m_1 + \epsilon X_i$ and $m_2^i = m_2 + \epsilon X_i$ ($i = 1, \cdots, n$; $n = 200$; $\epsilon = 0.1$; $m_1 = 1$; $m_2 = 2$; $K = 10$; $E_{\rm A} = 1$; $c_{\rm A} = 1$; $E_{\rm B} = 1$; $c_{\rm B} = 1$). The dashed lines indicate the limits of the pass-bands of the periodic system.

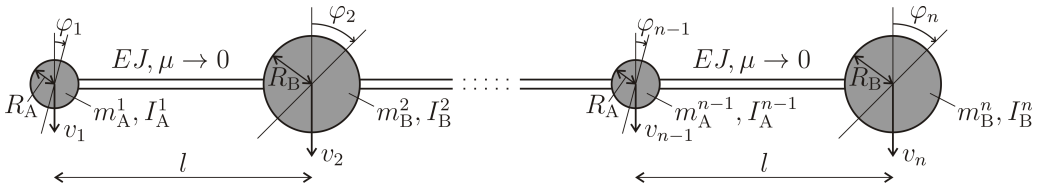

Figure 29: Discrete bi-coupled system made of two disks linked by massless beams (*bi-disk system*).

5. Discrete bi-coupled system with two types of disks

In this section, we examine a system consisting of two different types of disks connected by massless beams. This system, shown in Fig. 29, is hereafter referred to as *bi-disk system*. The radii of the two disks are indicated by R_A and R_B. Assuming that the density ρ_i ($i = 1, \cdots, n$) can vary, the masses and the rotational inertias of the two disks are given by $m_\mathrm{A}^i = \pi R_\mathrm{A}^2 \rho_i$, $m_\mathrm{B}^i = \pi R_\mathrm{B}^2 \rho_i$ and $I_\mathrm{A}^i = \pi R_\mathrm{A}^4 \rho_i/2$, $I_\mathrm{B}^i = \pi R_\mathrm{B}^4 \rho_i/2$, respectively.

The transfer matrix of each unit cell j ($j = 1, \cdots, n/2$) is given by the product of the transfer matrices (8) calculated with $R = R_\mathrm{A}$ and $R = R_\mathrm{B}$:

$$\mathbf{T}_j = \begin{bmatrix} \left(1 + \frac{m_\mathrm{B}^{2j}\omega^2 l^3}{6EJ}\right)\left(l - \frac{I_\mathrm{B}^{2j}\omega^2 l^2}{2EJ}\right) - \frac{l^3}{6EJ}\frac{l^2}{2EJ} \\ \frac{m_\mathrm{B}^{2j}\omega^2 l^2}{2EJ} \quad \left(1 - \frac{I_\mathrm{B}^{2j}\omega^2 l}{EJ}\right) - \frac{l^2}{2EJ}\frac{l}{EJ} \\ -m_\mathrm{B}^{2j}\omega^2 \quad 0 \quad 1 \quad 0 \\ m_\mathrm{B}^{2j}\omega^2 l \quad -I_\mathrm{B}^{2j}\omega^2 \quad -l \quad 1 \end{bmatrix} \begin{bmatrix} \left(1 + \frac{m_\mathrm{A}^{2j-1}\omega^2 l^3}{6EJ}\right)\left(l - \frac{I_\mathrm{A}^{2j-1}\omega^2 l^2}{2EJ}\right) - \frac{l^3}{6EJ}\frac{l^2}{2EJ} \\ \frac{m_\mathrm{A}^{2j-1}\omega^2 l^2}{2EJ} \quad \left(1 - \frac{I_\mathrm{A}^{2j-1}\omega^2 l}{EJ}\right) - \frac{l^2}{2EJ}\frac{l}{EJ} \\ -m_\mathrm{A}^{2j-1}\omega^2 \quad 0 \quad 1 \quad 0 \\ m_\mathrm{A}^{2j-1}\omega^2 l \quad -I_\mathrm{A}^{2j-1}\omega^2 \quad -l \quad 1 \end{bmatrix}. \tag{58}$$

The eigenvalues $\lambda = \omega^2$ of a finite bi-disk system are the solutions of the eigenvalue problem (10), where $\mathbf{X} = \{v_1, \varphi_1, v_2, \varphi_2, \cdots, v_{n-1}, \varphi_{n-1}, v_n, \varphi_n\}^T$ is the unknowns vector, $\mathbf{M} = \mathrm{diag}\left(m_\mathrm{A}^1, I_\mathrm{A}^1, m_\mathrm{B}^2, I_\mathrm{B}^2, \cdots, m_\mathrm{A}^{n-1}, I_\mathrm{A}^{n-1}, m_\mathrm{B}^n, I_\mathrm{B}^n\right)$ is the mass matrix and $\mathbf{K}$ is the stiffness matrix, which in the case of clamped ends is defined by Eq. (11). The reflected and transmitted energies are calculated from system (14), which was derived by assuming that a finite stack of n disks is placed between two homogeneous semi-infinite beams with flexural stiffness $\tilde{E}J$ and linear density $\tilde{\mu}$ (refer to the discussion in Section 2). Finally, the Lyapunov exponents are computed by following the procedure leading to Eq. (21).

In Section 5.1 we will analyse the bi-disk system with uniform density, while in Section 5.2 we will show how the dynamic properties of the system change if the density is perturbed randomly.

5.1. Ordered bi-disk system

Here we assume that $\rho_i = \rho$ for $i = 1, \cdots, n$. Accordingly, $m_{\mathrm{A}}^{2j-1} = m_{\mathrm{A}}$, $I_{\mathrm{A}}^{2j-1} = I_{\mathrm{A}}$, $m_{\mathrm{B}}^{2j} = m_{\mathrm{B}}$, $I_{\mathrm{B}}^{2j} = I_{\mathrm{B}}$ and $\mathbf{T}_j = \mathbf{T}$ for $j = 1, \cdots, n/2$.

The dispersion curves of a periodic bi-disk system, obtained from Eq. (22), are plotted in Fig. 30a in the normalised coordinates $\Omega = \omega\sqrt{m_{\mathrm{A}} l^3/EJ}$ and kl. In this case, there are four branches, indicated by ω_1-ω_4, because there are two types of disks with two degrees of freedom each. The superior branch ω_4 is dominated by rotations, while the inferior branch ω_1 is mainly characterised by translations. The motion associated with the branches ω_2 and ω_3 is instead a combination of rotations and translations.

The (normalised) eigenfrequencies of a finite bi-disk system with clamped ends are reported in Fig. 30b. All the eigenfrequencies fall within the Pass-Stop regions of the periodic system, except four of them, which are associated with localised eigenvectors (see the insets of Fig. 30b). We remind that the appearance of localised eigenstates in a perfect system is due to the chosen boundary conditions.

The reflected and transmitted energies are shown in Figs. 30c and 30d, respectively. In these figures, the functions $\mathcal{R}(\Omega)$ and $\mathcal{T}(\Omega)$ are plotted in different scales because the energy transmitted through the system at higher frequencies is very small, but still different from zero. Indeed, we note that $\mathcal{T} \simeq 0$ and $\mathcal{R} \simeq 1$ only within the Stop-Stop regions of the periodic system.

Fig. 30e presents the variation of the localisation factor (i.e. the smallest positive Lyapunov exponent) with the normalised frequency Ω. As expected, $\gamma_2 \simeq 0$ in correspondence of the Pass-Stop zones of the periodic system, while $\gamma_2 > 0$ elsewhere. On the other hand, the largest Lyapunov exponent $\gamma_1 > 0$ at any frequency, since one flexural wave always decays exponentially in space.

5.2. Disordered bi-disk system

Now we consider the situation in which the density of the disks is varied randomly, in particular $\rho_i = \rho + \epsilon X_i$ $(i = 1, \cdots, n)$, where ϵ is a small parameter and the variables X_i have a normal distribution as in Eqs. (29).

The (normalised) eigenfrequencies of a finite random system with clamped ends are shown in Fig. 31a, where the dashed lines represent the limits of the Pass-Stop zones of the periodic system, which are almost coincident with the limits of the eigenfrequency intervals of the perfect finite system (compare Figs. 30a and 30b). It is apparent that the spectrum of the perturbed system is larger than that of the perfect system. Nonetheless, all the eigenvectors

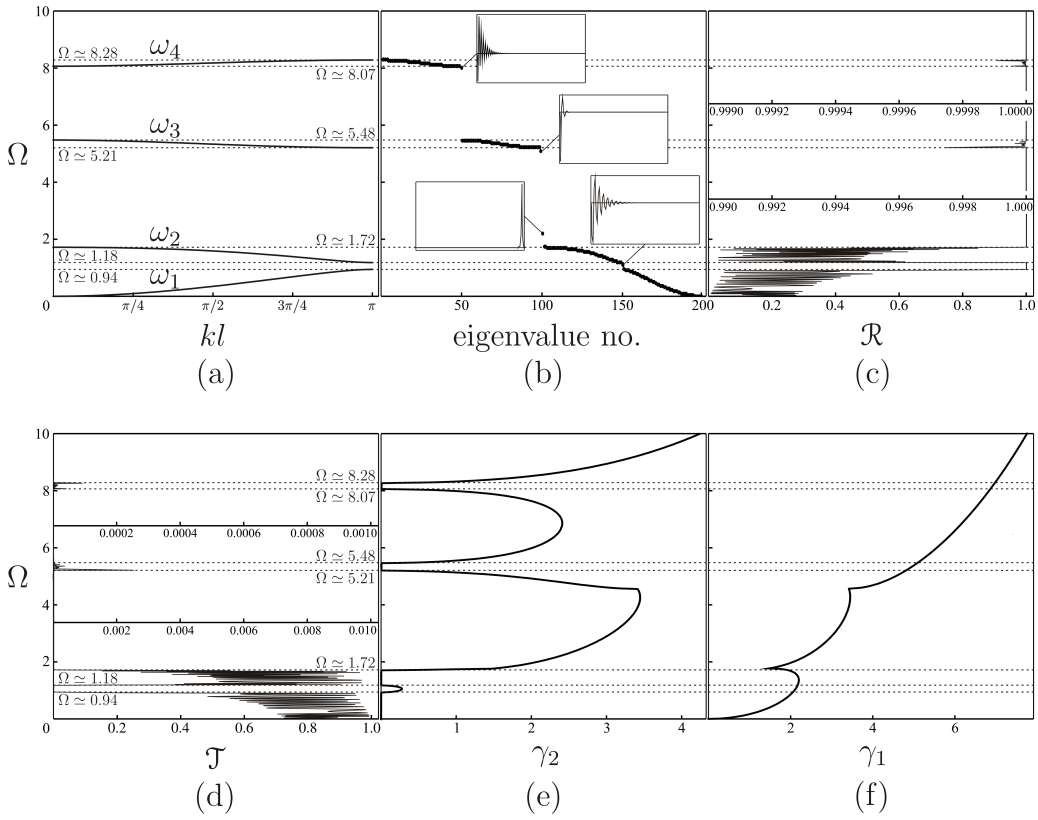

Figure 30: (a) Dispersion curves of a periodic bi-disk system; eigenfrequencies and localised eigenvectors(b), reflected energy (c), transmitted energy (d), localisation factor (e) and largest Lyapunov exponent (f) for a finite system with $n = 100$ disks ($\rho = 1$, $R_{\mathrm{A}} = 0.5$, $R_{\mathrm{B}} = 1$, $EJ = 10$, $l = 1$, $\tilde{EJ} = 1$, $\tilde{\mu} = 1$).

relative to the eigenfrequencies belonging to the two upper clusters are localised. Other localised eigenvectors are observed near the boundaries of the two lower clusters.

In order to determine the frequency ranges where waves can propagate through the finite system, we compute the reflected and transmitted energies, plotted in Figs. 31b and 31c. For $\Omega > 1.6$ all the energy is reflected back by the stack of disks. Indeed, all the eigenstates corresponding to normalised eigenfrequencies $\Omega > 1.6$ are localised. Therefore, the third and fourth propagation ranges of the finite system become non-propagation regions if the density of the disks is perturbed randomly. The same conclusion is drawn by looking at Fig. 31d, which shows that the localisation factor $\gamma_2 > 0$ for $\Omega > 1.6$.

While randomness reduces propagation in correspondence of the boundaries of the pass-bands of the periodic system, it decreases the decay rate of the corresponding evanescent waves in the periodic system, as can be noticed for example by comparing the local maxima in Figs. 30e-f and in Figs. 31d-e.

6. Conclusions

In this work, we have examined discrete elastic systems with uniform and random parameters. These are bi-coupled systems, made of translational and rotational masses connected by non-inertial beams. We have demonstrated that, in terms of dispersion properties, bi-coupled systems can be approximated by mono-coupled spring-mass models, provided that the rotational inertia of the masses of the bi-coupled systems is sufficiently small, as in the current engineering practice.

For each system, we have studied two problems. The *spectral problem* concerns the computation of the eigenfrequencies and eigenvectors of a finite stack. The *transmission problem* is focussed on the evaluation of energy transmission. In the randomly-perturbed structure we have detected localised modes, in particular near the limits of the propagation ranges and at high frequencies. We have shown that, while randomness expands the frequency spectrum of the ordered structure (a result that can be considered counterintuitive), the frequency intervals corresponding to energy propagation shrink. Furthermore, eigenfrequencies in the non-propagation regimes are associated with localised eigenstates, which indicates that a finite amount of energy is confined within a sub-region of the randomly-perturbed structure and it cannot propagate from one boundary to the other. Such result

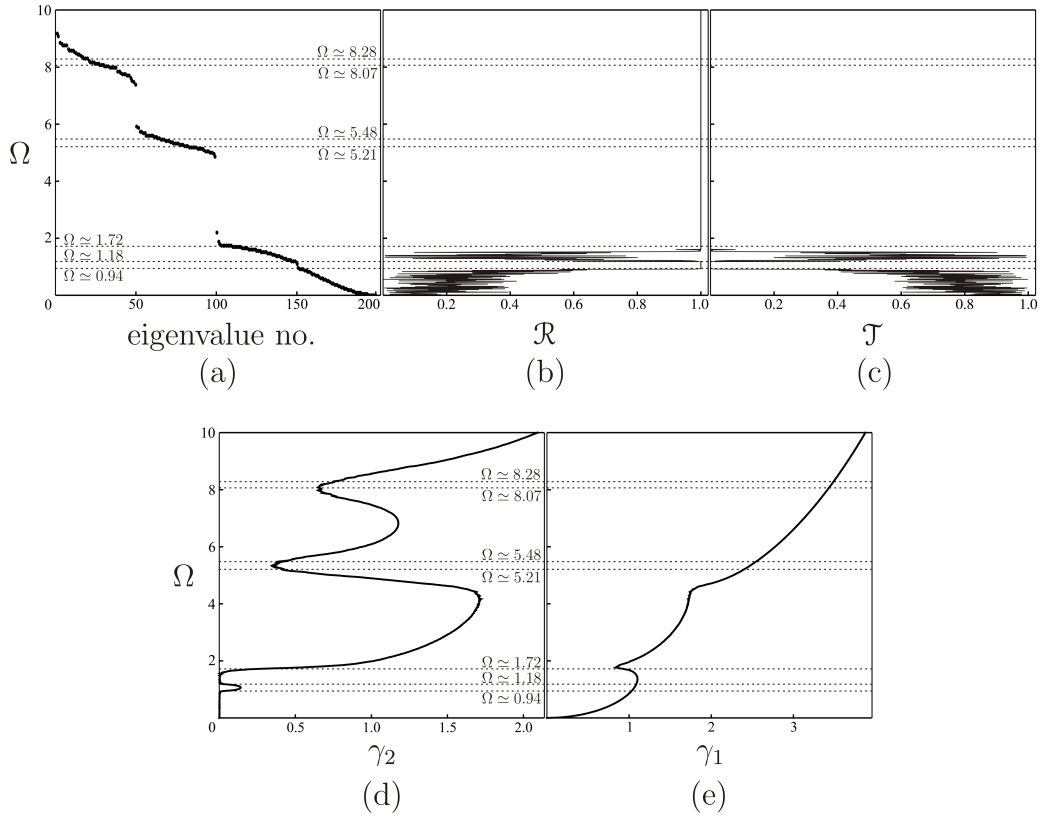

Figure 31: Eigenfrequencies (a), reflected energy (b), transmitted energy (c) and Lyapunov exponents (d,e) for a finite perturbed bi-disk system with random density $\rho_i = \rho + \epsilon X_i$, where X_i are defined by Eqs. (29) ($n = 100$, $\epsilon = 0.1$, $\rho = 1$, $R_{\rm A} = 0.5$, $R_{\rm B} = 1$, $EJ = 10$, $l = 1$, $\tilde{EJ} = 1$, $\tilde{\mu} = 1$). The dashed lines indicate the limits of the Pass-Stop regions of the periodic system (see Fig. 30).

is in contrast with the case of ordered structures, where resonance modes correspond to peaks in transmission. The introduction into the structure of heterogeneous sub-regions with uniform or randomly-perturbed properties confirms that reduction of the propagation frequency intervals is mainly due to randomness. Conversely, sub-regions with uniform properties have a strong influence on the generation of localised modes (this problem will be further studied in the future with the aim to maximise energy storage). We have also shown that the type of random distribution (normal, exponential and Gamma) strongly affects propagation ranges and frequency spectra. Finally, paradigmatic examples of bi-disk and bi-atomic structures highlight the possibility of fine-tuning propagation intervals by properly coupling regular and randomly-perturbed structures.

The results of this paper suggest that random perturbations can be deliberately introduced into the system to stop the transmission of waves of specific frequencies, thus creating a filter for elastic waves or a vibration shield. In this respect, we envisage new methodologies to design dynamically-optimised civil engineering structures, like arrays of tanks in industrial plants. Enhanced localisation can also be exploited to store the energy in confined regions of the structure. The procedures developed in this work could be extended to study higher-dimensional media, for which however a significantly larger computational cost would be required.

Acknowledgments

G.C. and A.B.M. acknowledge the Research Fund for Coal and Steel of the European Commission, INDUSE-2-SAFETY project, grant number RFSR-CT-2014-00025. G.C. and M.B. acknowledge the financial support of Regione Autonoma della Sardegna (LR7 2010, grant 'M4' CRP-27585).

References

Anderson, P.W. (1958). Absence of diffusion in certain random lattices. Physical Review, 109, 1492-1505.

Anderson, P.W. (1985). The question of classical localization. A theory of white paint? Philosophical magazine B, 52, 505-509.

Ariaratnam, S.T., & Xie, W.-C. (1995). Wave localization in randomly disordered nearly periodic long continuous beams. Journal of Sound and Vibration, 181, 7-22.

Asatryan, A.A., Botten, L.C., Byrne, M.A., Freilikher, V.D., Gredeskul, S.A., Shadrivov, I.V., McPhedran, R.C., & Kivshar, Y.S. (2012). Transmission and Anderson localization in dispersive metamaterials. Physical Review B, 85, 045122.

Asatryan, A.A., Gredeskul, S.A., Botten, L.C., Byrne, M.A., Freilikher, V.D., Shadrivov, I.V., McPhedran, R.C., & Kivshar, Y.S. (2010). Anderson localization of classical waves in weakly scattering metamaterials. Physical Review B, 81, 075124.

Bendiksen, O.O. (2000). Localization phenomena in structural dynamics. Chaos, Solitons and Fractals, 11, 1621-1660.

Borland, R.E. (1963). The nature of electronic states in disordered one-dimensional systems. Proceedings of the Royal Society A, 274, 529-545.

Bouzit, D., & Pierre, C. (2000). Wave localization and conversion phenomena in multi-coupled multi-span beams. Chaos, Solitons and Fractals, 11, 1575-1596.

Brillouin, L. (1953). Wave propagation in periodic structures: Electric filters and crystal lattices. New York (New York): Dover Publications.

Brun, M., Giaccu, G.F., Movchan, A.B., & Movchan, N.V. (2012). Asymptotics of eigenfrequencies in the dynamic response of elongated multi-structures. Proceedings of the Royal Society of London A, 468, 378-394.

Brun, M., Giaccu, G.F., Movchan, A.B., & Slepyan, L.I. (2014). Transition wave in the collapse of the San Saba Bridge. Frontiers in Materials, 1:12, 1-7.

Carta, G., & Brun, M. (2012). A dispersive homogenization model based on lattice approximation for the prediction of wave motion in laminates. Journal of Applied Mechanics, 79, 021019.

Carta, G., & Brun, M. (2015). Bloch-Floquet waves in flexural systems with continuous and discrete elements. Mechanics of Materials, 87, 11-26.

Carta, G., Brun, M., & Movchan, A.B. (2014). Dynamic response and localisation in strongly damaged waveguides. Proceedings of the Royal Society of London A, 470, 20140136.

Carta, G., Brun, M., & Movchan, A.B. (2014). Elastic wave propagation and stop-band generation in strongly damaged solids. Fracture and Structural Integrity, 29, 28-36.

Castanier, M.P., & Pierre, C. (1995). Lyapunov exponents and localization phenomena in multi-coupled nearly periodic systems. Journal of Sound and Vibration, 183, 493-515.

Cetinkaya, C. (1999). Localization of longitudinal waves in bi-periodic elastic structures with disorder. Journal of Sound and Vibration, 221, 49-66.

Chen, A.-L., & Wang, Y.-S. (2007). Study on band gaps of elastic waves propagating in one-dimensional disordered phononic crystals. Physica B, 392, 369-378.

Davies, E.B. (2007). Linear operators and their spectra. Cambridge (United Kingdom): Cambridge University Press, Cambridge studies in advanced mathematics, 106.

Dean, P., & Bacon, M.D. (1963). The nature of vibrational modes in disordered systems. Proceedings of the Physical Society, 81, 642-647.

Dyson, F.J. (1953). The dynamics of a disordered linear chain. The Physical Review, 92, 1331-1338.

Felbacq, D., Guizal, B., & Zolla, F. (1998). Limit analysis of the diffraction of a plane wave by a one-dimensional periodic medium. Journal of Mathematical Physics, 39, 4604-4607.

Furstenberg, H. (1963). Noncommuting random products. Transactions of the American Mathematical Society, 108, 377-428.

Godin, Y.A. (2005). Propagation of longitudinal waves in a random binary rod. Waves in Random and Complex Media, 16, 409-416.

Godin, Y.A., Molchanov, S., & Vainberg, B. (2011). The effect of disorder on the wave propagation in one-dimensional periodic optical systems. Waves in Random and Complex Media, 21, 135-150.

Gol'dsheid, Ya., Molchanov, S., & Pastur, L. (1977). Pure point spectrum of stochastic one dimensional Schrödinger operators. Functional Analysis and Its Applications, 11, 1-8.

Griffiths, D.J. (2004). Introduction to Quantum Mechanics. Upper Saddle River (New Jersey): Prentice Hall.

Guenneau, S., Movchan, A.B., Movchan, N.V., & Trebicki, J. (2008). Acoustic stop bands in almost-periodic and weakly randomized stratified media: perturbation analysis. Acta Mechanica Sinica, 24, 549-556.

Hundertmark, D. (2000). On the time-dependent approach to Anderson localization. Mathematische Nachrichten, 214, 25-38.

Ishii, K. (1973). Localization of eigenvalues and transport phenomena in the one-dimensional disordered system. Supplement of the Progress of Theoretical Physics, 53, 77-138.

John, S. (1991). Localization of light. Physics Today, May, 32-40.

Klein, A., & Koines, A. (2001). A general framework for localization of classical waves: II. Random media. Mathematical Physics, Analysis and Geometry, 4, 97-130.

Kunin, I.A. (1982). Elastic Media with Microstructure I - One-Dimensional Models. Berlin Heidelberg (Germany): Springer-Verlag, Springer Series in Solid-State Sciences, 26.

Kunz, H., & Souillard, B. (1980). Sur le spectre des opérateurs aux différences finies aléatoires. Communications in Mathematical Physics, 78, 201-246.

Lekner, J. (1994). Light in periodically stratified media. Journal of the Optical Society of America A, 11, 2892-2899.

Li, F.M., Wang, Y.S., Hu, C., & Huang, W.H. (2004). Localization of elastic waves in randomly disordered multi-coupled multi-span beams. Waves in Random and Complex Media, 14, 217-227.

Li, F., Wang, Y., Hu, C., & Huang, W. (2006). Wave localization in randomly disordered periodic layered piezoelectric structures. Acta Mechanica Sinica, 22, 559-567.

Lombardi, G., & Rebaudo, R. (1988). Eigenvalues and eigenvectors of a special class of band matrices. In Rendiconti dell'Istituto di Matematica dell'Università di Trieste, An International Journal of Mathematics, 20,

113-128. Trieste (Italy): Università degli Studi di Trieste, Dipartimento di Scienze Matematiche.

Martinelli, F., & Scoppola, E. (1985). Remark on the absence of absolutely continuous spectrum for d-dimensional Schrödinger operators with random potential for large disorder or low energy. Communications in Mathematical Physics, 97, 465-471.

Matsuda, H., & Ishii, K. (1970). Localization of normal modes and energy transport in the disordered harmonic chain. Supplement of the Progress of Theoretical Physics, 45, 56-86.

Maynard, J. (1988). Acoustic Anderson localization. In B.V. Kohn, & G.W. Milton (Eds.), Random Media and Composites (pp. 206-207). Philadelphia (Pennsylvania): SIAM.

Mead, D.J. (1975). Wave propagation and natural modes in periodic systems: I. Mono-coupled systems. Journal of Sound and Vibration, 40, 1-18.

Pastur, L.A. (1980). Spectral properties of disordered systems in the one-body approximation. Communications in Mathematical Physics, 75, 179-196.

del Rio, R., Jitomirskaya, S., Last, Y., & Simon, B. (1996). Operators with singular continuous spectrum, IV. Hausdor dimensions, rank one perturbations, and localization. Journal d'Analyse Mathématique, 69, 153-200.

Romeo, F., & Luongo, A. (2002). Invariants representation of propagation properties for bi-coupled periodic structures. Journal of Sound and Vibration, 257, 869-886.

Schmidt, H. (1957). Disordered one-dimensional crystals. Physical Review, 105, 425-441.

Sigalas, M.M., & Soukoulis, C.M. (1995). Elastic-wave propagation through disordered and/or absorptive layered systems. Physical Review B, 51, 2780-2789.

Trefethen, L.N., & Embree, M. (2005). Spectra and Pseudospectra: The Behavior of Nonnormal Matrices and Operators. Princeton (New Jersey): Princeton University Press.

Wolf, A., Swift, J.B., Swinney, H.L., & Vastano, J.A. (1985). Determining Lyapunov exponents from a time series. Physica D, 16, 285-317.

Yan, Z.-Z., Zhang, C., & Wang, Y.-S. (2009). Analysis of wave propagation and localization in periodic/disordered layered composite structures by a mass-spring model. Applied Physics Letters, 94, 161909.

Yao, W., Zhong, W., & Lim, C.W. (2009). Symplectic Elasticity. Singapore: World Scientific Publishing Company.